Republic of Iraq

Ministry of Higher Education

and Scientific Research

University of Anbar

College of Science

Department of Geology

Geological Implications of Crustal Structure in Central of Iraq Using the Receiver Function Technique

A Thesis

Submitted to the Council of College of Science - University of Anbar

in Partial Fulfillment of the Requirements of Master Degree in Geology

By

Huda Farhan Rafea

B.Sc. in Geology - College of Science - University of Anbar (2019)

Supervised by

Prof. Dr. Emad Abdulrahman Mohammed Salih
Department of Applied Geology, University of Anbar

Assist. Prof.Dr. Wathiq Gazi Abdulnaby
Department of Geology, University of Basrah

2022 A. D. 1443A.H

بسم الله الرحمن الرحيم

وَالنَّازِعَاتِ غَرْقًا (1) وَالنَّاشِطَاتِ نَشْطًا (2) وَالسَّابِحَاتِ سَبْحًا (3) فَالسَّابِقَاتِ سَبْقًا

(4) فَالْمُدَبِّرَاتِ أَمْرًا (5) يَوْمَ تَرْجُفُ الرَّاجِفَةُ (6) تَتْبَعُهَا الرَّادِفَةُ (7) قُلُوبٌ يَوْمَئِذٍ

وَاجِفَةٌ (8) أَبْصَارُهَا خَاشِعَةٌ (9) يَقُولُونَ أَإِنَّا لَمَرْدُودُونَ فِي الْحَافِرَةِ (10)

صدق الله العظيم

سورة النازعات

Supervisor Certification

I certify that the thesis entitled "**Geological Implications of Crustal Structure in Central of Iraq Using the Receiver Function**" has been made by **Huda Farhan Rafea** under my supervision in the department of Geology, college of Science, University of Anbar, in a partial fulfillment of the requirements for the Master Degree in Geology.

Signature:

Supervisor:

Scientific degree:

Date: / / 2022

In view of the available recommendations, I forward this thesis for debate by the examining committee.

Signature:

Name:

Scientific degree:

Date: / / 2022

Dedication

To

- Father's soul

-My mother is the greatest in the world who supported and encouraged me in my studies

-My brothers and sisters

-My teachers

-My friends

- Who helped me with anything with a word or effort.

Huda

Acknowledgements

I extend my deepest thanks and appreciation to my supervisors, **Prof. Dr. Emad Abdulrahman Mohammed Salih** and **Assist. Prof.Dr. Wathiq Gazi Abdulnaby** for suggesting the research project. Their follow-up in every step and their patience was the reason for the completion of this work.

My thanks and appreciation go to the Deanship of the College of Science represented by the Dean, and to the Presidency of the Department of Applied Geology represented by the Head of the Department and the Department's instructors.

Thanks and appreciation to my mother, brothers and sisters for their support and standing with me throughout the study stages.

I would like to extend my thanks and gratitude to the teacher, Osama Jassim Muhammad, the teacher in the Department of Applied Geology at the College of Science - University of Anbar.

My thanks and appreciation go to Mrs. Dhuha Muhammad for her valuable assistance during the research phase.

The family of Mr. Nofal Naji for standing with me throughout my studies.

Huda

Abstract

The current study aims to investigate the geological implications of the crustal structure beneath two seismic stations in central of Iraq. The inversion of the teleseismic P-wave receiver functions (RFs) was employed to determine the structure of the crust under Anbar (ANB1) and Karbala (KAR2) broadband seismic stations. Some of the computer programs in seismology (CPS) were used to analyze the receiver functions of seventeen teleseismic earthquakes.

Results of inversion show that the crustal thickness (Moho depth) beneath the study area ranges from 44 to 46km, with an average value of 45km. The sedimentary cover thickness (basement depth) in the study area is about 12km. In general, the obtained sedimentary cover and crustal thicknesses are consistent with the results of some previous studies in the Mesopotamian plain.

As well as the inversion results show that the crustal velocity model beneath the study area has four distinct layers; the first at 6km with Vs of 1.76 km/s, the second one at 12km with Vs of 2.84, the third one at 33km with Vs of 3.50 km/s, and the fourth one at 45km with Vs of 4.15km/s. The obtained velocity model may be employed to locate and relocate the local and teleseismic earthquakes and in moment tensor solutions.

The crustal thickness, Vp/Vs, and Poisson's ratios are important parameters that are used to understand the crustal structure, composition, deformation, and evolution. As mentioned above, the average crustal thickness of the study area is 45 km. The obtained crustal thickness value is consistent with that reported in the platform regions. The crustal Vp/Vs of the study area equals 1.79. This value is typical for the platform region and andesitic rocks. An intermediate value (0.27) of the crustal Poisson's ratio was reported. It indicates that there is little difference in the felsic and mafic contents of the crust.

List of Contents

List of Figures

List of Tables

Chapter One

Preface

Earth's Crust is the thinnest and the most primary layer that makes up the Earth. The crust is referred to as a chemical layer that has varying chemical compositions and it is divided into two types, the continental crust and oceanic crust (Nawaz, 2019). The crust preserves a record of the Earth's evolution. The geophysical methods are used to determine the crustal structure. The best and the most effective techniques are the seismic methods. There are two types of seismic techniques: active seismic sources and passive seismic sources (seismic refraction and reflection techniques). The techniques that use passive seismic sources include surface wave dispersion studies, seismic tomography, and seismic receiver functions. Because it just takes a single broadband seismic station, teleseismic receiver functions is an extremely efficient technique for exploring the seismic crustal structure. The P-wave receiver functions analysis yields the seismic velocity model beneath the seismic station.

In seismology, the seismic velocity of the continental crust represents the beginning point for a broad range of research (Kelly *et al.,* 2007). The reliable local and teleseismic locations depend on the local and regional seismic velocity structure (Chiu *et al.,* 1997). The seismic velocity structure of the continental crust can be also used in moment tensor solutions. The accuracy of the seismic velocity model is vital to the success of moment tensor solutions (Robertson,2008). Earthquake moment tensor solutions give useful information for understanding active tectonics and stress fluctuations (Pondrelli *et al.,* 2002). In relation to seismology, crustal structural models define differences in physical characteristics which can be used to model tectonic processes and the development of continental lithosphere (Kelly *et al.,* 2007).

A recent studies employed the receiver function to investigate crustal structure beneath the seismic stations (e.g Ramthan *et al.*,2020; Abdulunaby *et al.,* 2020; Yu and Hua,2021; Vervaet and Darbyshire,2022; Chi *et al.*,2022 and Chen *et al.*,2022). According to the most recent above studies, the method is still a useful and inexpensive for studying the crust in locations where seismic stations are available

In Receiver function technique the teleseismic body waveforms is used image the crustal structure underneath isolated seismic stations. These wave contain informations related to the source time function, Propagating effect through the mantle and local structures underneath the recording site. The resulting receiver function is obtained by removing the effects of the source and mantle path effects.

1.1. Literature Review

1.1.1 Global Literature Review

Zhu and Kanamori (2000) used teleseismic receiver functions to study the Moho depth difference in southern California. They estimated that the average of Moho depth in Southern California is 29 kilometers, with a range of 21 to 37 kilometers. The Vp/Vs ratio average in Southern California crust equals to 1.78, with exception of the ECSZ, where the ratio rises, greater ratios of 1.8 to 1.85 are found in mountain ranges with Mesozoic basement and lower ratios in the Mojave Block.

Torian (2003) used the receiver functions analysis to study the crustal structure of Cuba derived. The author found clear layering at some sits with a Moho depth ranging between 18-31 km. The velocity models show an upper mantle P-wave between 7.6 and8.0 km/sec.

Ottemoller and Midzi (2003) studied the crustal structure of Norway using inversion teleseismic receiver functions. They found that Moho depths are ranging between 28 - 44 km. The P velocities in the crust indicate a progressive increase from about 6.0 to 7.1 km/sec at most locations.

Chang and Baag (2005) studied a joint analysis of teleseismic receiver function and surface-wave dispersion to determine the crustal structure in southern Kora. They suggested that the range of Moho depth is from 26 to 36 km. Average crustal velocities in Southern Korea ranged from 6.02 km/sec to 6.51 km/sec.

Hetenyi and Bus (2007) employed receiver function inversions at four permanent stations in Hungary to evaluate the Pannonian basin's shear wave velocity and crustal thickness. They found Moho at depths of 27 to 34 km. The Poisson s' ratio increased in the study area.

Mitra *et al.,* (2008) estimated the crustal structure of the western Bengal basin using the teleseismic receiver function and surface-wave dispersion analysis. The Moho was discovered at a depth of 37.5 km. The average S-wave velocity in the crust is 3.7 km/sec.

Zhou *et al.,* (2009) studied the crustal velocity structure underneath the Yanqing-Huailia Basin NW of Beijing inferred using the teleseismic receiver function and surface –wave. They found that the total crustal thickness is 38-42 km with a smooth Moho to an upper mantle Vs=4.3 km/sec.

Chen *et al.,* (2010) analyzed the receiver function to determine the crustal structure underneath China. They calculated a Moho depth of 51 kilometers along with the Tian Shan fold system and 84 kilometers beneath the Tibet Plateau's central region. Over the mainland China crust, the average value of the Vp/Vs ratio equals 1.730.

Taghizadeh *et al.,* (2010) used P and S receiver functions to deduce the lithospheric structure of NW Iran. They showed an average Moho depth of 48 km. The average of the Vp/Vs ratio was estimated to be 1.76.

Kieling *et al.,* (2011) studied the velocity structure beneath the N Sumatra and the Malaysian peninsula inferred using the receiver function. Near the surface, they found that the ranges of Moho depth and Vs are 30-34 km and 3.4-3.6 km/s, respectively.

Motaghi *et al.,* (2012) employed the teleseismic converted waves to estimate the crustal thickness variation across the NE Iran continental collision zone. They found a large variance in Moho depth, ranging from 27.5 kilometers under central Iran to 55.5 kilometers beneath the Binalud foreland basin. The thickest crust is not found beneath the Kopeh Dagh and Binalud mountain ranges' high topography, implying that these mountain ranges are not supported by a crustal root.

Grad and Tiira (2012) used teleseismic receiver functions to investigate the Moho depth of the European Plate. They discovered that the uncertainty is about 2 km for a 20-km -thick crust and about 4 km for a 60-km-thick crust. The Moho depths indicate an approximately the values are roughly identical for the Moho depth of 30–40 km.

Saikia *et al.,* (2017) used a receiver function to estimate the crustal structure and geological implications of the SW edge of NE India. They found the crust is thicker (38-45 km) in the Tripura fold and the depth of the sediments in the Bengal basin is up to 8 km on its eastern margin. The Vp/Vs ratio is between 1.69 and 1.75.

Badawy *et al.,* (2018) used joint inversion of receiver function and surface wave dispersion to investigate the crustal structure of northern Egypt. They found that crustal thickness ranges from east to west, with a maximum of 36 kilometers in the western desert and a minimum of 28 kilometers at the Sinai Peninsula's southernmost station, Sharm. In northern Egypt, the Vp/Vs ratio ranges from 1.71 to 2.07, while in the SAW station, it is 1.93.

Kalmár *et al.,* (2019) estimated the Moho depth beneath the eastern Pannonian basin and the southern Carpathians using the receiver function. They showed that the Apuseni mountains had the thickest crust (28-32 km), the southern Carpathians had the deepest Moho (33-43 km), the AlCaPa and Tisza-Dacia blocks had the shallowest Moho depths (22-28 km), and the eastern Pannonian basin had the shallowest depths.

Zhang *et al.,* (2019) used principal component analysis of receiver functions to investigate crustal structure. They found that the existence of two roughly parallel dipping discontinuities inside the crust can best explain the RF data. They interpreted the shallow dipping discontinuity as the top boundary of the Precambrian crystalline basement of the Sichuan Basin and the deep one as the interface between the upper and lower crust, based on previous logging data, seismic exploration, and deep sounding observations, which is consistent with the geological feature of the study area.

Alkan *et al.,* (2019) investigated the crustal and upper-mantle structure of the eastern Pontides orogenic region (NE, Turkey) using the receiver function. From east to west, they discovered crustal thicknesses of 30, 33, 37, and 40 km, with Moho depths of 46, 42, 39, and 44 km, respectively, under the southern stations. The inversion data from the northern area provide crustal models that show a low P and S wave velocity (Vp = 5.0 km/s and Vs = 2.8 km/s) indicating the uppermost crust.

Ortega and D'Auria (2021) studied the crustal structure of Tenerife using the receiver function. They suggested that the Moho topography has a gentle slope beneath the volcanic edifice, with varying depths from 11 to 18 km. Further, some phases associated with a layer of volcanic rocks with a thickness of about 5.5 km and a P-wave velocity (Vp) of around 6 km/s, and they found that have been discovered a top an old oceanic crust with a thickness of about 7 km and a Vp of roughly 6.8 km/s

Yu and Hua (2021) investigated the geological aspects of Crustal thicknesses and Vp/Vs ratios determined using receiver function analysis beneath South China. They reported that crustal thicknesses range from 25 km in the east to 46 km in the research area. The higher Vp/Vs ratios is about 1.77~1.86 under the southeastern Cathaysia block indicate a primarily intermediate-to-mafic crust.

Vervaet and Darbyshire (2022) used receiver function analysis to deduce the structure of the crust near the boundaries of the eastern Superior craton in Canada. At depths of 33–46 km, they found that stations on Archean terranes possessed a fundamental crustal structure with a well-defined Moho 46–55 km depth. Except for a station located in an area dominated by anorthosite massifs, where the bulk crustal composition is much more mafic (Vp/Vs 1.85), the bulk crustal composition is primarily felsic to intermediate (Vp/Vs 1.66–1.76) over the whole region.

Chi *et al.,* (2022) used receiver function Imaging of the crustal structure beneath Northern Taiwan using Dense Linear Arrays. They showed The Eurasian Plate's Moho depth in west Taiwan is flat and 30 km. The crustal structure appears to be thin at these Moho depths. In the west region of northern Taiwan, the terrain is flat and similar to the thin-skin concept.

The lithosphere, on the other hand, is deformed in the east and produces the mountain root, which is comparable to the lithospheric collision concept.

Chen *et al.,* (2022) studied the crustal thickness and composition in the South China Block using the receiver function. The Cathaysia Block, Jiangnan Orogenic Belt, and Yangtze Block all had markedly distinct crustal structures and Vp/Vs ratios. The average depth of the Moho in the Cathaysia Block was approximately 31 km and the Vp/Vs ratios ranged from 1.66 in the inland area to 1.78 in the coastal area. The crustal thickness of the Jiangnan Orogenic Belt increases from the east (31km) to the west (42km), with Vp/Vs ratios ranging from 1.75 to 1.64, indicating a felsic crust.

1.1.2. Local Literature Review

Al-Heety, E. (2002) studied the crustal structure of the northern Arabian platform at Rutba station and Baghdad station using the spectral ratio method. The author suggested a crustal model including three distinct layers and Moho discontinuity depth of 36.5 km and a velocity of 7.8 km/sec for the upper mantle are indicated. The crustal model shows that the crust consists of three distinct layers with P-velocities ranging from 6.0 to 6.6 km/sec.

Abdulunaby *et al.,* (2012) used receiver function and surface wave dispersion to investigate the crustal structure under Duhok, NW Iraq. They found two different discontinuities, one at a depth of 18-20 km and the other at a depth of 42-44 km, both with shear wave velocities of 4.05 km/sec.

Abdullah and Abdulunaby (2020) studied the crustal structure of southern Iraq inferred using cross-correlation of ambient seismic noise. They found the sedimentary thickness is around 10 km (Vs 1.995 -2.48 km/sec). The Moho discontinuity is located around 41 km.

Ramthan *et al.,* (2020) used receiver function analysis to determine the crustal velocity model under the Al-Refaei seismic station in central Mesopotamia. They found a crustal model with two discontinuities: the basement depth of 8 km with Vs of 2.63 km/sec and the Moho depth of 46 km with Vs of 3.79 km/sec.

Abdulunaby *et al.,* (2020) investigated the crustal structure of the Mesopotamian plain based on teleseismic data from 12 new seismic stations. A combination of P-wave receiver function inversion and Rayleigh wave dispersion data was utilized to determine S-wave velocity structure models underneath each station. They discovered that the Moho is steadily rising in the research region, from the Arabian platform to the Zagros mountains, with a particularly deep root near Mesopotamia's eastern boundary.

From our review of the above studies we find that the common method to investigate crustal structure in Iraq was the receiver function which we will use in our study.

1.2. Geological Implications

1.2.1. Crustal Parameters

Many active, passive seismic, and potential field investigations have found that understanding the nature and tectonic regime evolution inside the Earth's crust requires knowledge of Moho sharpness, Vp/Vs, and crustal thickness (Mooney *et al.,* 1998; Gao *et al.,* 2004; Wei *et al.,* 2011; Keller, 2013). Crustal formation, structure, and evolution are constrained by crustal thickness, Vp/Vs ratio, and Moho intensity (Zhu and Kanamori, 2000; Chen *et al.,* 2010; Liu and Gao, 2010).

1.2.1.1. Crustal Thickness

The thickness of the crust varies between tectonic zones, with the continental crust being 30-70 kilometers thick and the oceanic crust being 6-17 kilometers thick, according to global measurements. (Tewari and Kumar, 2018). The average crustal thickness of major tectonic provinces is 40.77 ± 7.04 km (Shield), 42.66 ± 10.56 km (Orogeny), 31.33 ± 8.27 km (Arc), 39.96 ± 7.03 km (Platform), 30.54 ± 6.03 km (Extended crust), and in Fore arc is 26.78 ± 7.88 km (Mooney *et al.,* 1998).

Tectonic distortion, thermal expansion, the injection of surface volcanic materials, the placement of magmatic intrusion deeper within the crust, and sedimentation all contribute to crust thickening (Yang and Liu, 2009). Because the lower crustal layer is ductile during deformation, the crust becomes thicker predominantly in the lower layer of the crust during orogeny (Condie ,2011).

The crust thins due to internal crustal processes. These activities include the following: Lateral movements include cooling of lithosphere or change of phase, surface erosion after thermal uplift, ductile flowage, subcrustal erosion, dense material injection, magma chamber collapse, and rifting and transverse shearing (Buck ,1991; Thybo and Nielsen ,2008).

1.2.1.2. Vp/Vs Ratio

The results of laboratory experiments and seismic refraction/reflection exploration have been proven that the Vp/Vs ratio is more beneficial than either Vp or Vs solely (Zandt and Ammon, 1995; Christensen, 1996). The Vp/Vs ratio can be used to determine the crustal composition and tectonic evolution (Liu and Gao, 2010; Nwe *et al.,* 2021). The Vp/Vs ratio provides important information about the continental crust's physical characteristics (Saikia *et al.,* 2017).

The Vp/Vs ratio is tied closely to crustal composition (Chen *et al.,* 2010; Saikia *et al.,* 2017). Poisson's ratios (σ) determined from field measurements provide valuable constraints on crustal composition (Christensen,1996) because the correlation between Vp and composition is limited due to the similar P-wave velocities of many common crustal rock types (Christensen and Mooney,1995). Vp/Vs ratio is significantly associated with quartz and feldspar proportions in the crust as an essential physical characteristic that directly related to Poisson's ratio (σ) (Zhang *et al.,* 2021).

The Vp/Vs ratio value decreases with the increase of silica content, in other words, the felsic rocks reduce the Vp/Vs value in the crust, while the mafic/ultramafic rocks (high content of Fe and Mg) increase the Vp/Vs value in the crust (Zandt and Ammon,1995; Christensen, 1996; Ji *et al.,* 2009). The Vp/Vs value of granitic rocks is 1.71, 1.78 for andesitic rocks and 1.87 for basaltic rocks (Tarkov and Vavakin, 1982). The e crustal Vp/Vs average value is 1.78 and ranges from 1.74 in the upper layer of the crust to 1.81 in the lower layer (Christensen, 1996). The fluid content and partial melt lead to an increase in the Vp/Vs value (Watanabe, 1993). Extensive melting results in a high Vp/Vs ratio (> 1.87), (Chevrot and Van der Hilst, 2000; Nwe *et al.,* 2021).

There is a strong relationship between the crustal Vp/Vs average and the type of the crust (Zandt and Ammon ,1995). In the Precambrian shield and platform, the average Vp/Vs values

are 1.84 ± 0.005 and 1.78 ± 0.01, respectively (Zandt and Ammon, 1995; Christensen, 1996). The Vp/Vs value is lower (0.01-1.73) but more changeable in Mesozoic–Cenozoic orogens, indicating lithologic and temperature fluctuations in the early orogenic crust (Zandt and Ammon 1995; Christensen, 1996). They were exceptionally high along subduction zones, as a result of the presence of water, most likely (Audet *et al.,* 2009). Under the Tibetan plateau and Myanmar, the Vp/Vs ratio was found to be exceptionally high. This observation was explained in terms of the occurrence of the fluid content and partial melting of the crust (Xu *et al.,* 2007; Nwe *et al.,* 2021). The Vp/Vs ratio in volcanic locations is larger than usual due to magma chambers and volcanic lava (Koulakov *et al.,* 2011).

1.3. Relationships between crustal parameters

The relationships between crustal parameters, crustal thickness, crustal average Vp, and Vp/Vs ratio have been investigated by many researchers.

1.3.1. Relation between Vp and crustal thickness

For the stable continental crust, a relationship between crustal thickness and mean crustal velocity was suggested by Wever and Sadowiok (1989). They found that mean crustal velocity increases with increasing the crustal thickness and this relation was interpreted in terms of the crustal growth due to accretion from below

1.3.2. Relation between Vp/Vs ratio and the crustal thickness

There is no straightforward link between crustal thickness, Vp/Vs ratio, and crustal thickness (Chen *et al.,* 2010). Many previous receiver function studies show that geological regions of different ages and tectonic history can be distinguished by the relationship Vp/Vs ratio and crustal thickness. In Precambrian Cratons, the Vp/Vs ratio is proportionate to crustal thickness, but in the Cenozoic Basin and Paleozoic fold belts, it is inversely related to crustal thickness (Egorkin, 1998). The Yangtze Block in the South China Block has a positive association between average crustal thickness and Vp/Vs ratios, which is explained by the comparatively thick mafic lower crust (Chen *et al.,* 2022). In the eastern South China Block, crustal thickness and average Vp/Vs ratios are inversely associated. This relationship is viewed as demonstrating tectonic thickening of the felsic upper and middle crust during

orogeny, as well as probable mafic lower crust delamination (Zhang *et al.*, 2021). The tectonic thickening of the felsic upper crust will lead to a decrease in Vp/Vs ratio with increasing crustal thickness, while the addition of mafic material through basaltic underplating will increase in Vp/Vs ratio with increasing crustal thickness (Zhang *et al.*, 2021). In the Western United States, there is no apparent association between crustal thickness and the Vp/Vs ratio value in the crust underlying the various tectonic provinces (Uranbaigal, 2014).

1.3.3. Relation between Vp/Vs ratio and age of the crust

The Vp/Vs ratio increases with crust age, according to Zandt and Ammon (1995). The comparison result of different crustal models from many parts of the world showed that in general, Proterozoic terrans have a thicker crust than the Archean (Durrheim and Mooney, 1994). The difference, they concluded, is related to the presence or absence of a several kilometers lowermost mafic layer. The relationship between crustal age and Vp/Vs is highly controversial, according to Vp/Vs data from throughout the world (Chen *et al.*, 2010). The crust of the eastern Zimbabwe and southern Kaapaval Cratons in southern Africa is thin (approximately 38km) and has a low Vp/Vs ratio (about 1.73) (Niu and James, 2002; Nair *et al.*, 2006). The Vp/Vs ratio variations in different tectonic regions of the Australian crust were investigated by Chevrot and Van der Hilst (2000). They showed that for the Proterozoic crust, the Vp/Vs ratio grows with increasing crustal thickness, but for the Phanerozoic crust, it decreases with increasing crustal thickness. The mean value of Vp/Vs ratio for southern Africa and Australian Cratons is 1.74 and 1.76, respectively ((Niu and James, 2002; Nair *et al.*, 2006; Chevrot and Van der Hilst, 2000). These mean Vp/Vs values are much lower than the global value of 1.84 for shields and platforms (Zandt and Ammon, 1995). In the Western of United States, Uranbaigal (2014) found that there is no clear relation between Vp/Vs ratio and crustal age.

1.4. Crustal Layers

On the criterion of seismic wave velocity, the continental crust has been classified into two to four layers (Hacker *et al.*, 2015). According to Hacker et al. (2011), there are two layers termed upper crust with a thickness of 14 km and lower crust of 26 km. Huang et al. (2013)

divided the continental crust into three layers: the upper crust of 13km thickness, the middle crust of 11km thickness, and the lower crust of 10km thickness. Rudnick and Gao (2014) divided Earth's crust into three layers- upper crust, middle crust, and lower crust. Upper, middle, and lower crust layers have thicknesses of 12, 11, and 17 km, respectively. The fourth (lowermost crust) layer is generally thin or absent (Nawaz, 2019). At a specific site, these layers may have a clear geological meaning; for example, a huge sedimentary basin may be an upper crustal layer with characteristic wave velocity (Hacker *et al.*, 2015).

1.5. Continental crust composition implications

The continental crust preserves the majority of the Earth's geological, physical, and chemical development. The formation of the continental crust, and at what rates and models, is a fundamental subject in the earth sciences community. It is commonly known that the majority of today's continents are made up of rocks formed between the end of the Archean and the beginning of the Proterozoic, around 3.2 to 2.0 Ga. (Stein and Ben-Avraham, 2015).

The continental crust shares a large amount of major and trace element composition with andesites at active continental edges. The belief that andesitic magmatism through oceanic subduction zones under continental plates played a crucial role in the development of continental crust along the convergent plate boundaries arose from this result. (e.g. Rudnick, 1995; Kelemen, 1995; Wedepohl, 1995). The current continental crust has an overall andesitic composition, with niobium (Nb) depletion relative to lanthanum (La), (Rudnick and Gao, 2003).

Convergent margin magmatism is the commonly recognized mechanism for the formation of the continental crust. Much of today's continental formation takes place near convergent plate boundaries, primarily along subduction zones. Two notes about this mechanism are reported, firstly, several investigations have found that significant quantities of continents were formed in the geological past during periodic super events at speeds that are difficult to explain using regular subduction rates (Stein and Ben-Avraham, 2015), and secondly, the disparity in the chemical composition of the crust and the primary mantle melts could not be explained by convergence margin magmatism (Rudnick and Gao, 2003).

Many authors have been dedicated their studies to petrogenesis of andesities in the past two decades (e.g. Annen *et al.*, 2006; Streck *et al.*, 2007; Tatsumi *et al.*, 2008; Reubi and Blundy, 2009; Kent *et al.*, 2010; Castro *et al.*, 2013; Straub *et al.*, 2014; Chen *et al.*, 2016; Gómez-Tuena *et al.*, 2018; Chen *et al.*, 2021).

Gómez-Tuena *et al.*, (2014) classified several models for peterogenesis of andesites into two primary categories: basalt-input model and andesite-input model. The importance of basaltic magma differentiation is supported by the basalt-input model, while the role of source mixing between the mantle wedges and the subducting crust is confirmed by the andesite-input model.

Several processes have been introduced to explain the chemical differences between the main mantle melts and the current crust's composition (Rudnick, 1995; Kelemen, 1995). These processes include (1) mafic/ultramafic lower crust upper mantle delamination, (2) crust production from a mixture of silicic melts from subducted oceanic crust and basaltic melts from peridotite, and (3) crust weathering, with preferential recycling of Mg ± Ca into the mantle via hydrothermally altered mid-ocean ridge basalt (Albarede, 1998).

The processes mentioned above reveal that mafic to ultramafic rocks return to the convecting mantle, and their lithologies constitute the chemical supplement of today's andesitic crust. (Rudnick and Gao, 2003).

A common characteristic of convergent margin magmas is the significant depletion of niobium (Nb) compared to lanthanum (La) in the crust (Kelemen et al., 2003). According to the degree of Nb depletion found in the crust, at least 80% of the crust was created in a convergent margin (Barth *et al.*, 2000).

Chen *et al.*, (2021) revealed that their findings not only support the hypothesis that the trace element and radiogenic isotope composition of andesite can be directly produced by source mixing and mantle melting but also show that partial melting of basaltic metasomatities can produce the lithochemical composition of andesites. It was also shown that andesites petrogensis may not need to recall the large contributions from magma differentiation or crustal contamination.

1.6. Location of the study area

The study areas include Ramadi and Karbala cities. Ramadi is located in west Iraq between the of latitudes (33° 25′ 33.5" N) and longitudes (43° 17′ 59.7" E). Karbala is in central Iraq, between longitudes (44 º 45' – 43 º 09' E) and latitudes (33º 32' 42" 31º 47' 24" N) Figure.1.

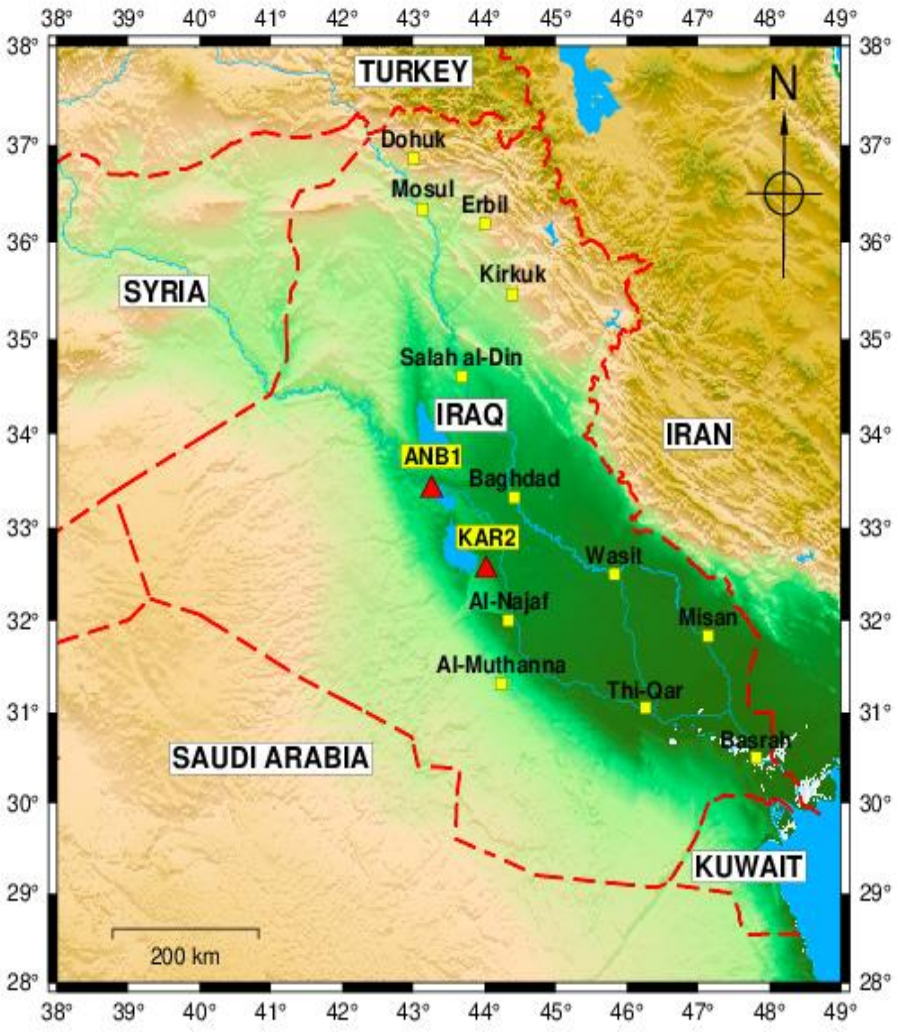

Figure 1-1: Location of the ANB1 and the KAB2 seismic stations. The red triangles are the seismic stations. The yellow squares are the locations of the main cities.

1.7. Tectonic and Geological setting area

The Arabian Shield and Platform regions comprise the Arabian Shelf. Iraq is located inside the platform region, and the Arabian shelf Iraqi part is divided into two sections: stable and unstable shelf. The area of study is within the Stable Shelf. The Stable Shelf is a tectonically stable monocline that has been mostly undamaged by Late Cretaceous and Tertiary deformation. The geometry of the underlying basement blocks and faults, Palaeozoic epirogenic processes, and Mesozoic arching all influenced the orientations of the structures in this tectonic unit. From west to east, the Shelf is presently divided into three major tectonic zones: The Rutba-Jezira, Salman, and Mesopotamian Zones. The study area is located on the stable continental shelf area's western edge of the Mesopotamian zone (Jassim and Goff, 2006). The Mesopotamian zone is divided into three longitudinal units: The Zubair zone, Euphrates zone, and Tigris zone. The Euphrates subzone, where the study area is located, is the shallowest unit in Mesopotamia Figure.2, but the Quaternary sediments are thicker than those in the Tigris subzone. The Abu- Jir fault zone is a major structural feature in the studied region, as well as an underlying fault that extends from north to south (Sissakian and Muhamad, 1994). The study area is rather flat from a geomorphological standpoint and gradually increases to the west, except in the northwestern part of the study area, where the slope is gradually gently toward the north (Yass *et al.*, 2016).

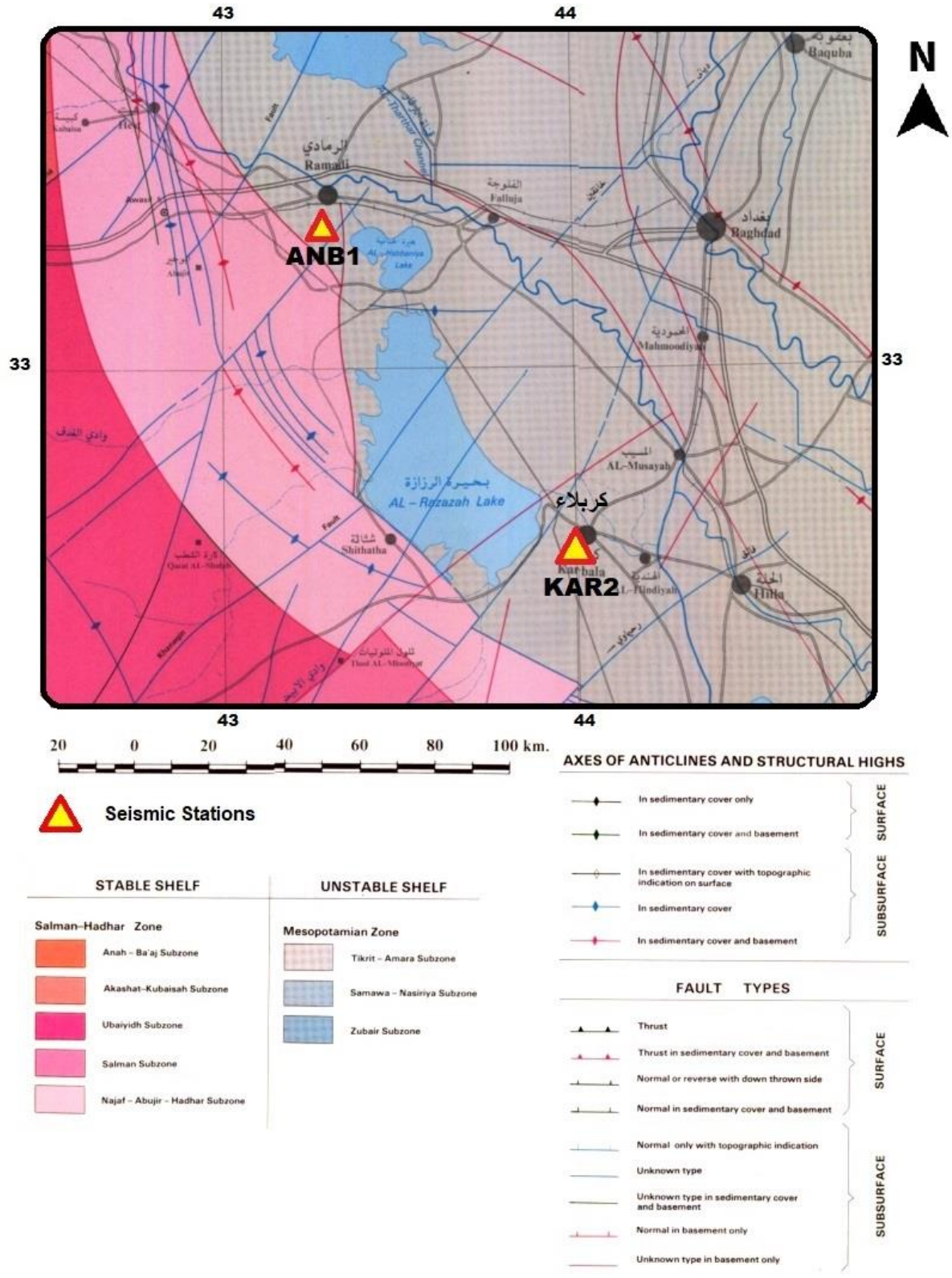

Figure.1-2: Tectonic map of the study area (Al Kadhimi *et al.*, 1996)

The sediments and geologic sequence of the study area, from oldest to youngest units (Hussien,2012).

- Fatha Formation (Middle Miocene): It is one of Iraq's most widely spread and economically important formations. It's composed of anhydrite, gypsum, and salt, with limestone and marl interspersed.
- Dibdibba Formation (Middle Miocene): It is made up of sand and gravel with volcanic rock pebbles (including pink granite) and white quartz, which is typically formed into a hard grit. Wells in the Nahr Umr field have recorded beds of limestone, marl, and silt.
- Injana Formation (Late Miocene): It is composed of fine-grained pre-molasse sediments that were first deposited in coastal areas and then later in a fluviolacustrine system. The majority of this formation is made up of different colored sand and clay rocks (Green, grey, and brown).
- Quaternary Deposits: These deposits, which extend to the Euphrates river and include sand, shale, clay, and gravel in some areas, are outcropped in Salah Aldin & Al-Anbar governorate, with Pleistocene sediments in the northern half of the analyzed region. as we come closer to the Euphrates River, the thickness of these deposits alters, and their density increases.

1.8. Problem of the study

The lack of information related to the structure of the earth's crust in the study area. The presence of two seismic stations (ANB1 and KAR2) in the study area motivated us to use the receiver function technique in determining the crustal structure beneath these stations and extraction of the geological implication of the crustal structure.

1.9. Aim of the study

1. Analyses of the receiver function beneath the ANB1 and KAR2 seismic stations in central of Iraq to estimate the crustal structure.
2. Investigation of the geological implication of crustal structure beneath the study area using the crustal thickness, Vp/V and Poisson's ratio.

Chapter Two

Data and Method

2.1. Receiver Functions Analysis

One of the techniques used to study the earth's crust is receiver functions (RFs) analysis. Teleseismic P-waves, which provide information on the crustal structures beneath a single station, are the central principle of the receiver function technique. Depending on the nature of the contact and the wave's incident angle, wave energy may be transmitted, reflected, or converted in this instance. As a result, the receiver functions technique is a time series acquired by the three components of a seismometer that provide the Earth's corresponding change in the structure of the crust beneath a seismic station (Stein and Wysession, 2003). Moho boundary is one of the interactions that body waves contact with it. Over this border, the velocity of both P and S waves varies significantly. Teleseismic waves propagate spherically in all directions when an earthquake occurs. The P and S waves will contact the Moho boundary and go further into the crust, where the seismometer will record it as a P-wave. The P-wave will arrive at the seismic station as direct P and Ps waves especially given the fact that a portion of it will be turned into an S-wave and then traveled (Ammon, 1991). Figure (2-1) shows the P, PpPs, PsPs,and PpPs that are the reflected waves employed in the receiver functions technique.

The basic concept of receiver functions analysis is shown to be dependent on: (1) the velocity difference of P and S waves across the Moho boundary, (2) the diversion of the P phase into the S phase at the crust-mantle interface, and (3) the multiple reflections of the diverted P-to-S phases resonance in the crust that are recorded at the seismic station (Stein and Wysession, 2003).Decomposing a vertical component of a teleseismic P wave into its horizontal components yields receiving functions (Langston, 1979). A Gaussian filter is employed to eliminate high frequencies, and a water-level parameter is used to ensure deconvolution stability (Langston, 1979; Ammon,1991). The water-level value was set to 0.01, and the Gaussian filter parameter was set to 2.5, resulting in an effective high-frequency limit of around 0.5 Hz in the P-wave data.

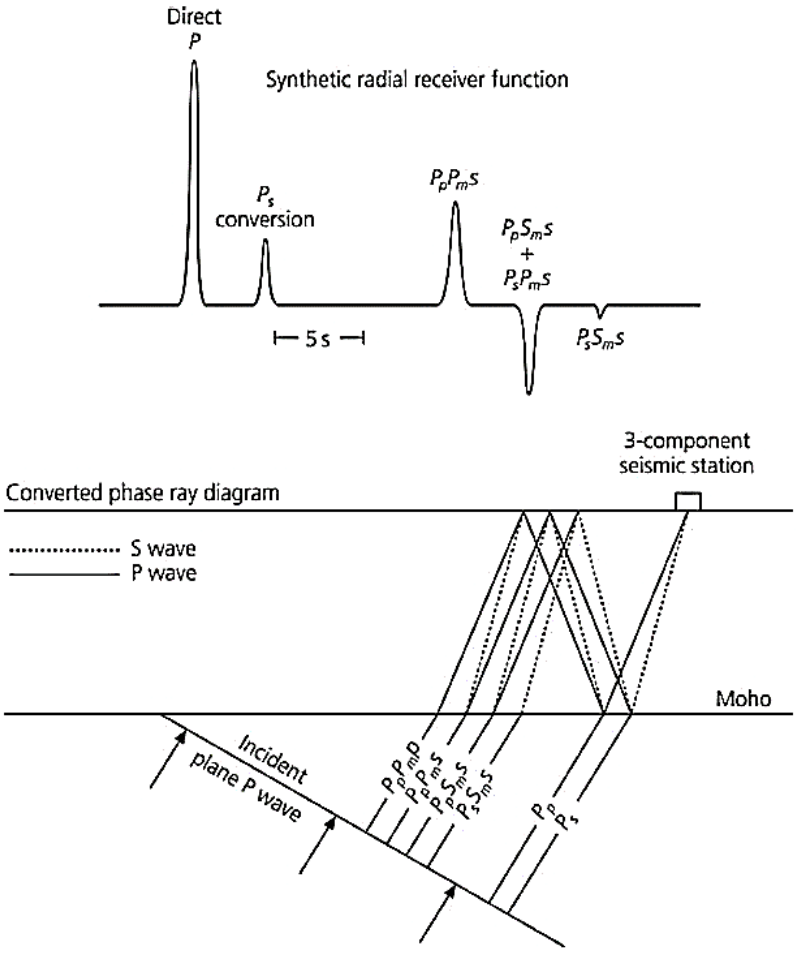

Figure 2-1: A description of the receiver function technique for determining crustal structure beneath a single station. The arrivals and following reverberations are depicted in the upper panel. The ray trajectories in a one-layer model for particular altered phases are shown in the lower panel, along with the associated arrival times isolated by the receiver function (top) (Stein and Wysession, 2003).

Herrmann and Ammon (2002)'s Computer Programs in Seismology (CPS) version 3.30 was used in this project and was installed on a LINUX platform. The CPS is a software bundle that includes over 140 scriptable programs. These programs assist the user in studying and interpreting seismic wave propagation in the Earth's crust and mantle. The software tools allow for the inversion of surface-wave dispersion and teleseismic P-wave receiver functions to determine the crustal structure. The CPS package can be found at http://www.eas.slu.edu/eqc/eqccps.html .

The last version of CPS prepared by Herrmann (2013) was used to analyze the receiver function of the teleseismic earthquake recorded by the seismic station of the study area. The CPS is a collection of more than 155 applications that may be launched interactively or using shell scripts on the Linux platform.

The Generic Mapping Tools (GMT), which is the most common software used in seismology, was used to plot all the maps in this study. The GMT is developed and maintained by Paul Wessel and Walter Smith in 1988 and has undergone several major enhancements since then (Wessel *et al*., 2019). The GMT is available at http://gmt.soest.hawaii.edu/ (last accessed May 2022), and it is installed on a LINUX platform. Different GMT scripts were used to provide the maps in this study.

2.2. Data Preparation

The receiver function method is dependent on a set of requirements to be met in order to accurately image the Earth's interior. A large magnitude is one of these criteria, as it ensures a high signal-to-noise ratio. To ensure the arrival of usable propagation pathways, the event must be located between 30^0 and 90^o from the seismic station (Rondenay, 2009). As a result, the events from the ANB1 and KAR2 seismic stations with magnitudes more than 7 Mw and epicentral distances of 30^o to 90^o were chosen as appropriate events for this study. The events information (date, origin time, latitude, longitude, magnitude, and focal depth) was extracted by the open access to metadata of the European-Mediterranean Seismological Centre (EMSC). It also allows performing customized searching within the database for a certain region.

In this research, the two seismic stations were selected as ANB1 in western and KAR2 in central Iraq, the search was limited to the period from 2018 to 2021. ANB1 and KAR2 seismic stations are part of the Mesopotamian Network (MP), University of Basrah. At three components digitizers, the ANB1and KAR2 seismic stations are provided with CMG40T/DM24 broadband seismometers. The crustal structure beneath the ANB1 and KAR2 seismic stations was determined using the method of inverting P-wave receiver functions.

Due to the high ambient noise and the difficulty of selecting the first P wave interval, many of the earthquakes recorded by two seismic stations were removed from the data set, and thus not all of them could be used. Seventeen remote events matching the above criteria were obtained, and the receptor function analysis method was applied. Table (2-1) lists the identified earthquake data. Figures (2-2 and 2-3)show the distribution of specific earthquake events. As a result, the crustal discontinuities and depths of the research region beneath the ANB1 and KAR2 seismic stations were determined using the P-wave receiver functions inversion approach.

Table 2-1. Earthquakes information that was used in the receiver functions inversion of the ANB1 and KAR2 seismic stations.

Date	Time (UTC)	LAT.	LON.	Depth (km)	Mw.
2018 12 29	03:39:09.740	5.89830	126.9209	60.21	7
2019 11 14	16:17:40.582	1.61990	126.414	33	7.1
2020 02 13	10:33:44.492	45.6313	148.9293	144	7
2020 03 25	02:49:20.896	48.9688	157.6914	55.39	7.5
2021 01 21	12:23:04.237	5.00540	127.5185	80	7
2021 02 13	14:07:50.838	37.7602	141.7196	51.89	7.1
*2021 03 20	09:09:44.002	38.4754	141.6328	43	7
2021 05 21	18:04:13.557	34.5884	98.2402	10	7.3
*202112 29	18:25:51.877	-7.5924	127.5808	166.92	7.3
2018 09 28	10:02:43.480	-0.1781	119.8401	10	7.5
2018 09 29	03:39:09.740	5.89830	126.9209	60.21	7
2019 06 24	02:53:39.830	-6.4078	129.1692	212	7.3
2020 02 10	10:33:44.492	45.6313	148.9293	144	7
2021 02 13	14:07:50.838	48.4756	141.7196	51.89	7.1
2021 05 21	18:04:13.557	34.5884	98.2402	10	7.3

*Two earthquakes recorded in the ANB1 and KAR2 stations

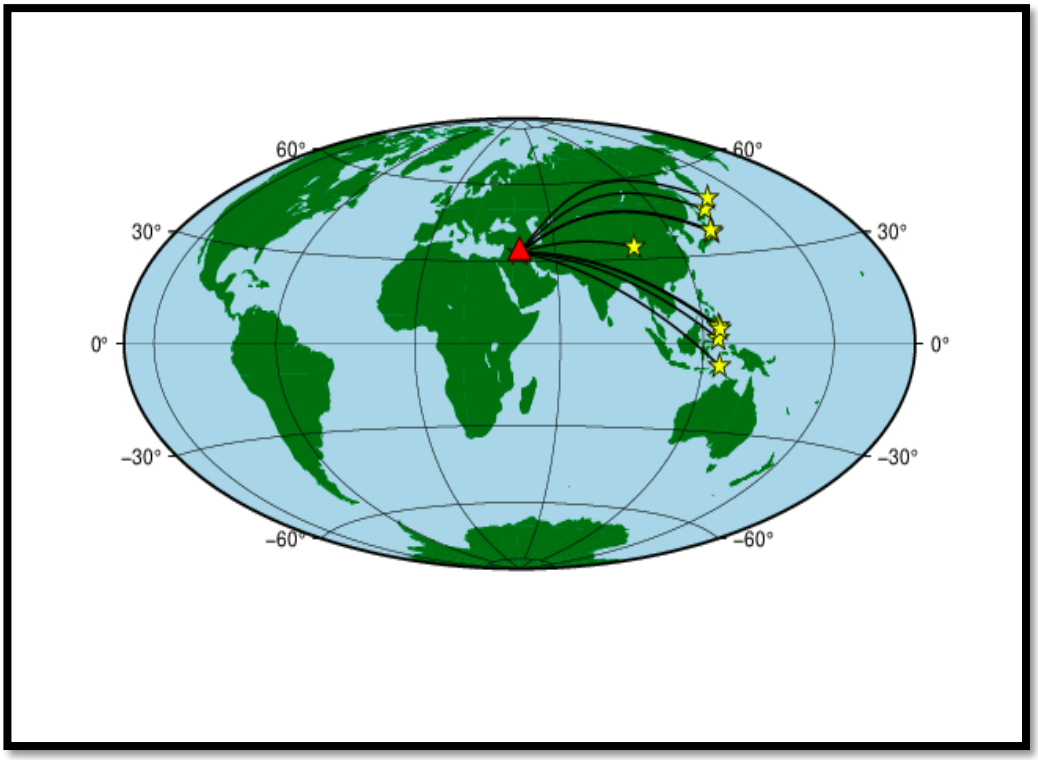

Figure 2-2: Earthquake distribution map recorded by ANB1 (red triangle). The yellow star symbol indicates the locations of the earthquakes.

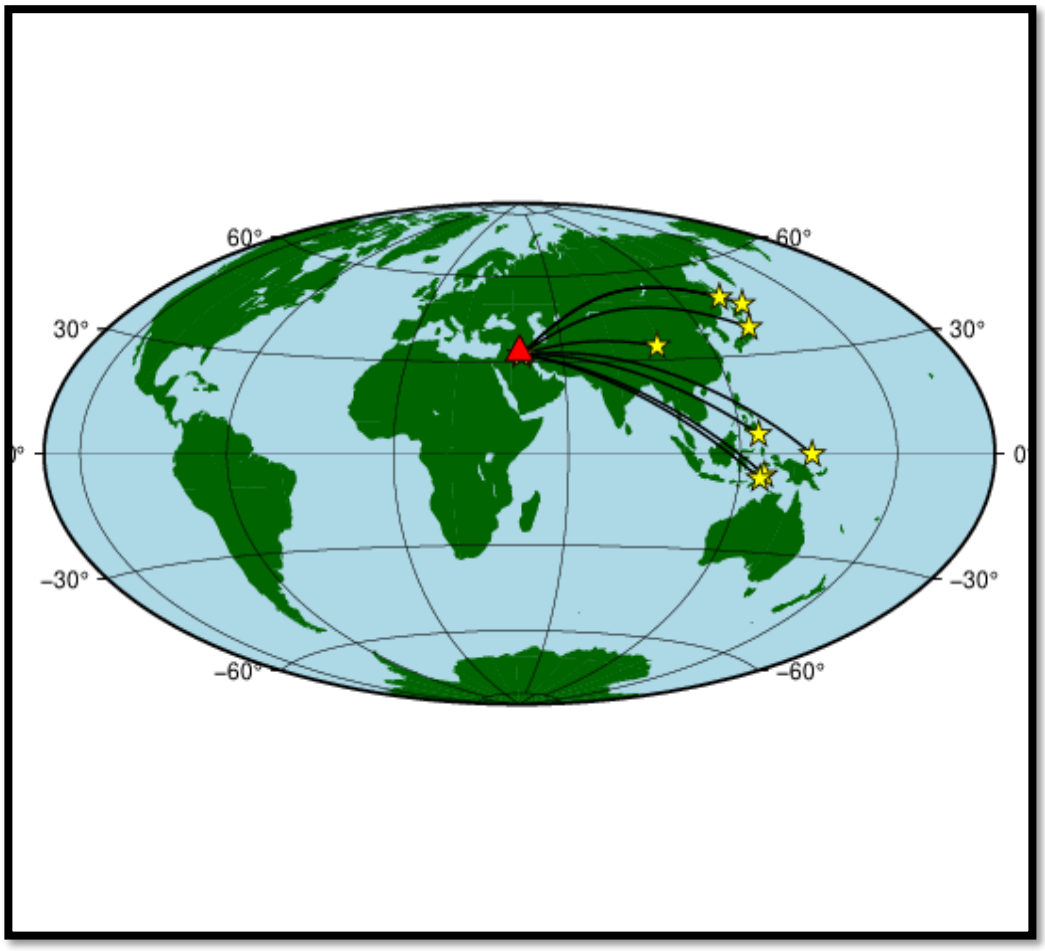

Figure 2-3: Earthquake distribution map recorded by KAR2 (red triangle). The yellow star symbol indicates the locations of the earthquakes.

2.3. Calculating Receiver Functions

Information on the source of the event, its propagation path across the mantle, and the localized structure underneath the station are all present in the teleseismic waves that arrive at the broadband seismic station. The receiver function method aims to extract the structure of the crust at the receiver by isolating it from the influence of crustal structure at the source and remote structure impacts (Shearer, 2009). The influence of source time functions and near-source structure were removed by the deconvolution method (Ligorria and Ammon, 1999).

P-wave radial receiver functions are radial waveforms formed by deconvolving the vertical and radial components of teleseismic P-waveforms to isolate receiver site impacts from other information (Langston, 1979). This approach has been demonstrated to be useful in determining crust thickness and Vp/Vs ratios beneath seismic stations (Zhu and Kanamori, 2000). For data processing and quality control, the following procedures we used: (1) the earthquakes occurrence was picked with the correct epicentral distances and magnitudes, (2) the time of arrival of the first P-wave from the event to the station was determined (3) the waveforms of the three components were manually analyzed. to ensure appropriate signal-to-noise ratios, events that made a lot of noise were removed, (4) the waveform record from the original Z, N, and E coordinate system were shifted to the Z, R (radial direction), T (transverse direction) coordinate system by rotating the coordinate system of the original recording components and (5) the receiver functions were extracted using a time domain deconvolution technique (Ammon, 1991).

The receiver function approach employs seismic station surface data to build a time series that concentrates on velocity variations across layers. The arrival times of converted phases at a discontinuity, such as the Moho, are transformed to depths to turn receiver functions. To convert seismic Earth velocities to depths, iterative inversion requires information on seismic Earth velocities. The S-wave velocity variance and discontinuities are the primary determinants of receiver functions (Abdulnaby, 2013). Starting with S-wave velocity (Vs) = 3.5 km/sec, the values for the receiver function were inverted using a homogeneous earth structure model termed half-space. For a depth of 400 km, the half-space depicts an initial velocity model with 65 layers. We employed 24 top layers in the investigation, each of which is 2 kilometers deep and has a constant velocity. The rftn96 program from the CPS package was used for the inversion technique. By minimizing the difference between actual and predicted receiver functions, this program relies on linearized-iterative inversion (Herrmann and Ammon, 2007). Each event was subjected to twelve iterations in order to develop the receiver functions.

The six panels exhibit the R and T components, which were filtered with three different Gaussian filters (0.5, 1.0, and 2.5 Hz). The radial and transverse components receiver functions of one of the selected events are shown in Figure (2-4). The receiver functions for the seventeen selected events that their epicentral distances extending from 30° to 90° are shown as a function of the back azimuth in Figures (2-5and2-6). The back azimuth number assists in identifying the alignment of events.

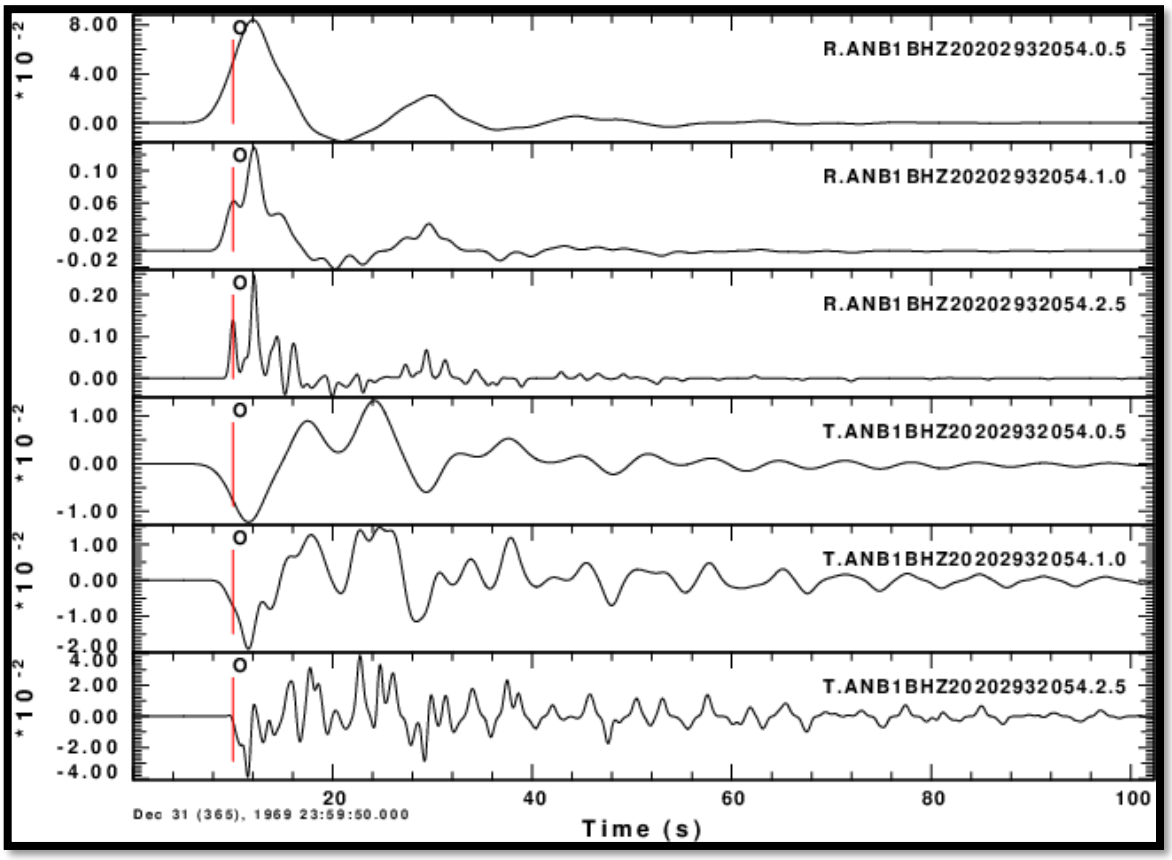

Figure 2-4: P-wave receiver function of the 2020/02/13 earthquakes (see Table 1). R and T represent the radial and transverse components filtered with three values 0.5, 1.0, and 2.5.

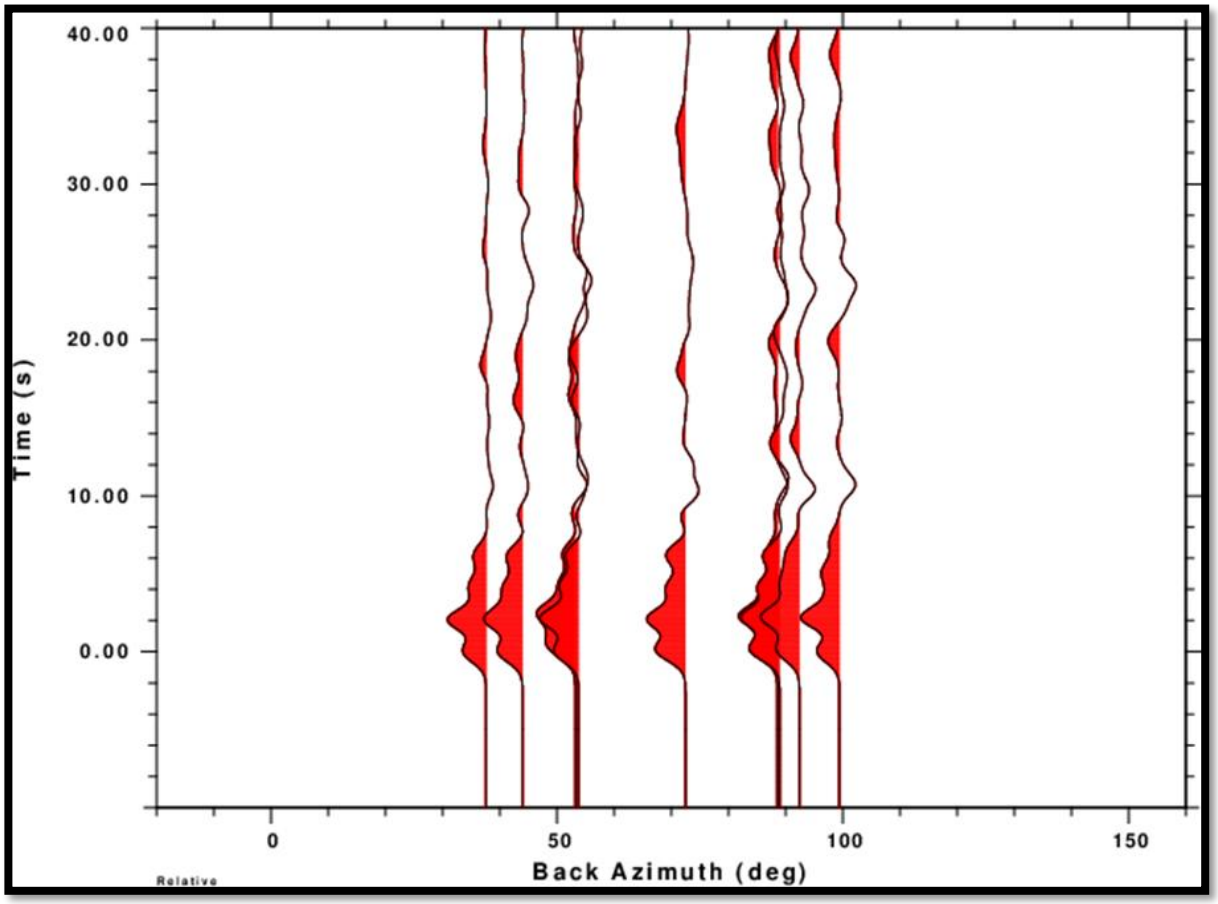

Figure 2-5: Receiver functions plotted as a function of back azimuth for 9 events recorded by the ANB1 station ranges from 30º to 90º. Overlapping one event with the four events shown.

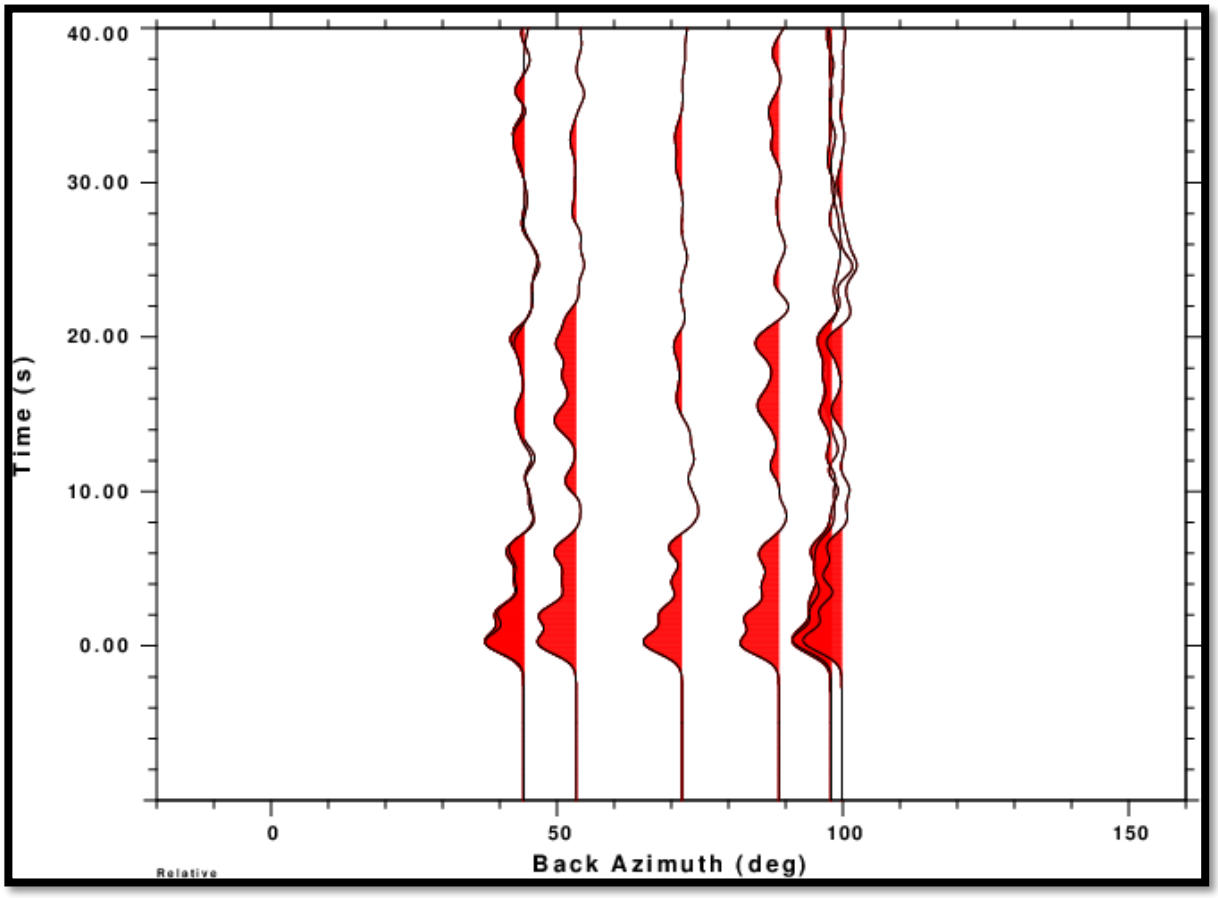

Figure 2-6: Receiver functions plotted as a function of back azimuth for 8 events recorded by theKAR2 station ranges from 30º to 90º. Overlapping one event with the four events shown.

2.4. Calculating Poisson's ratio

Poisson's ratio is the ratio of transverse strain to corresponding axial strain on a material stressed along one axis. Poisson's ratio is theoretically dependent on Vp/Vs. Depending on the results of inversion of receiver functions; the Vp/Vs ratio was calculated. The following equation was used to calculate Poisson's ratio (Christensen 1996):

$$\sigma = \frac{1}{2}\left[1 - \frac{1}{(Vp\ /\ Vs)^2 - 1}\right]$$

where σ is Poisson's ratio. It is dimensionless and ranges between 0 and 0.5. Most crustal rocks have Poisson ratios between 0.25 and 0.30. Although many different elastic parameters have been defined, it should be noted that two parameters (Vp and Vs) and density are sufficient to give a complete description of isotropic elastic properties (Shearer, 2009).

Chapter Three

Results and Discussion

3.1. Results

The inversion of the receiver function for seventeen earthquakes was used to estimate a crustal structure beneath the study area. Gaussian filter parameters equal to 0.5,1 and 2.5 were employed in the inversion of receiver functions. The best matching between the observed and theoretical receiver functions identifies the final velocity model. Results of the inversion receiver function are listed Table 3-1. The best velocity model beneath ANB1 seismic station which exhibited the best matching observed and theoretical receiver functions is shown in Figure (3-1). The crustal velocity model beneath the ANB1 station is shown in Figure (3-2) and the average crustal velocity model beneath the ANB1 seismic station is shown in Figure (3-3) and listed in Table 3-2.

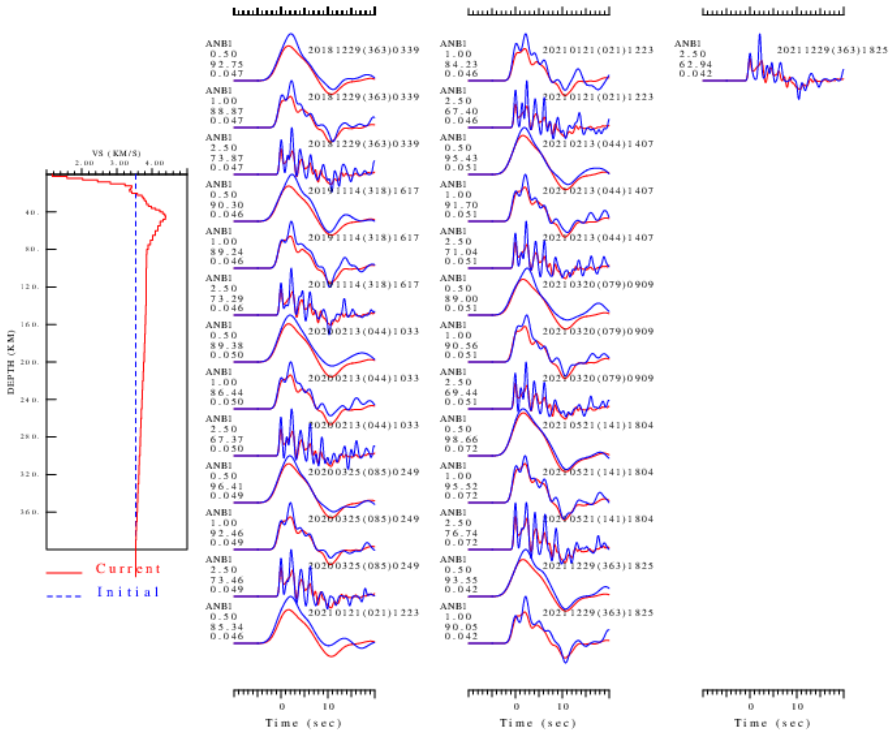

Figure 3-1: Model matching to the receiver functions of nine earthquakes recorded by ANB1. The blue curve shows the observed data and the red curve shows the model prediction.

Table 3-1. The crustal structure parameters beneath ANB1 and KAR2 seismic station.

Layer Thick (km)	ANB1			KAR2		
	Vp (km/sec)	Vs (km/sec)	ρ gm/cm^3	Vp (km/sec)	Vs (km/sec)	ρ gm/cm^3
2	1.9700	1.0989	2.3328	3.2215	1.7967	2.1893
2	2.7454	1.5312	2.0904	3.4027	1.8981	2.2166
2	3.6025	2.0094	2.2458	3.8563	2.1510	2.2945
2	4.5781	2.5535	2.4085	4.6774	2.6089	2.4285
2	5.5924	3.1193	2.6213	5.0610	2.8231	2.5115
2	6.4043	3.5721	2.8249	5.6612	3.1578	2.6305
2	6.4164	3.5788	2.8285	5.9441	3.3154	2.6876
2	6.3431	3.5379	2.8083	6.0782	3.3903	2.7215
2	6.3791	3.5579	2.8204	6.0472	3.3732	2.7151
2	6.5593	3.6587	2.8713	6.0808	3.3919	2.7236
2	6.8624	3.8277	2.9449	6.0316	3.3642	2.7080
2	7.0089	3.9092	2.9777	5.8672	3.2725	2.6736
2	6.9316	3.8663	2.9562	5.8832	3.2813	2.6772
2	6.8162	3.8017	2.9303	6.1297	3.4190	2.7364
2	6.7964	3.7909	2.9340	6.1976	3.4567	2.7550
2	6.9191	3.8596	2.9757	6.1881	3.4516	2.7545
2	7.0981	3.9593	3.0390	5.9680	3.3288	2.6958
2	7.2322	4.0339	3.0848	6.0807	3.3917	2.7273
2	7.3465	4.0977	3.1212	6.2658	3.4949	2.7855
2	7.4137	4.1350	3.1405	6.8781	3.8365	2.9520
2	7.4380	4.1487	3.1476	7.2366	4.0362	3.0598
2	7.4723	4.1678	3.1576	7.4932	4.1796	3.1389
2	7.5236	4.1962	3.1725	7.7458	4.3204	3.2210
2	7.5835	4.2299	3.1902	7.9151	4.4147	3.2772

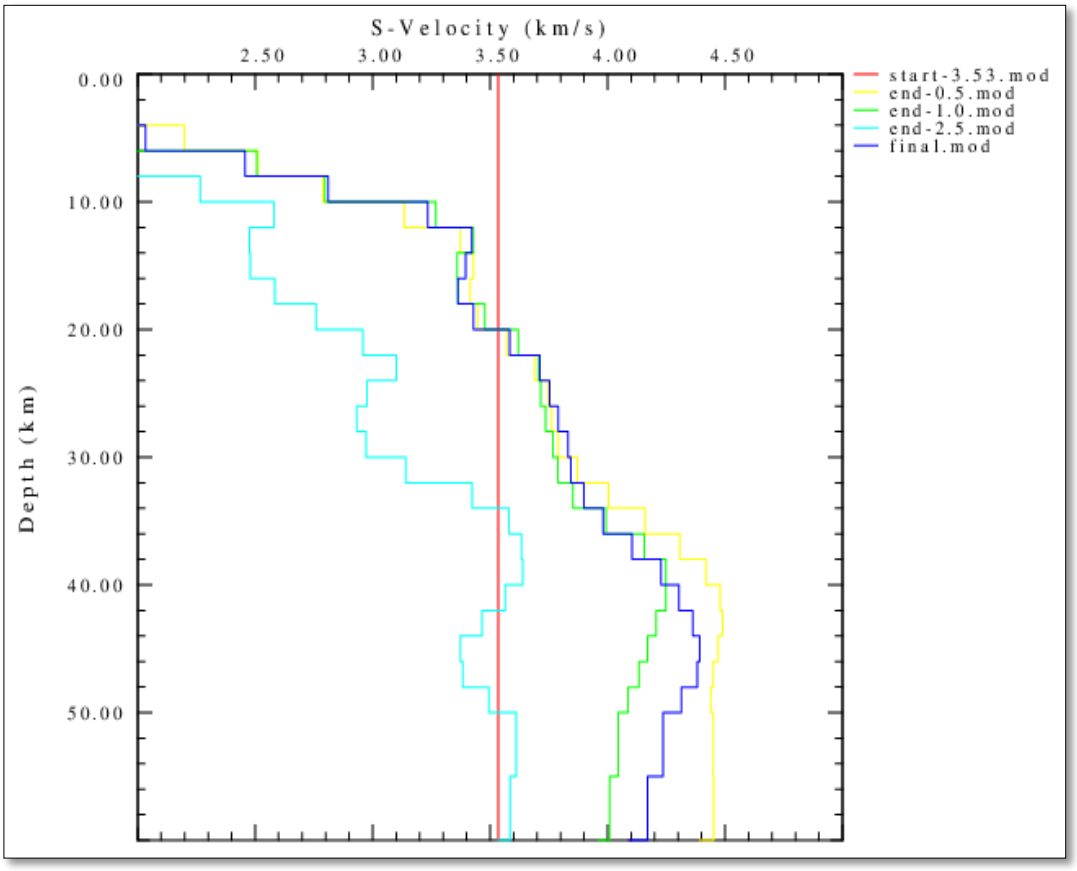

Figure 3-2: Velocity crustal model underneath ANB1 station. The red line is the starting velocity model. The blue line is the final Vs model

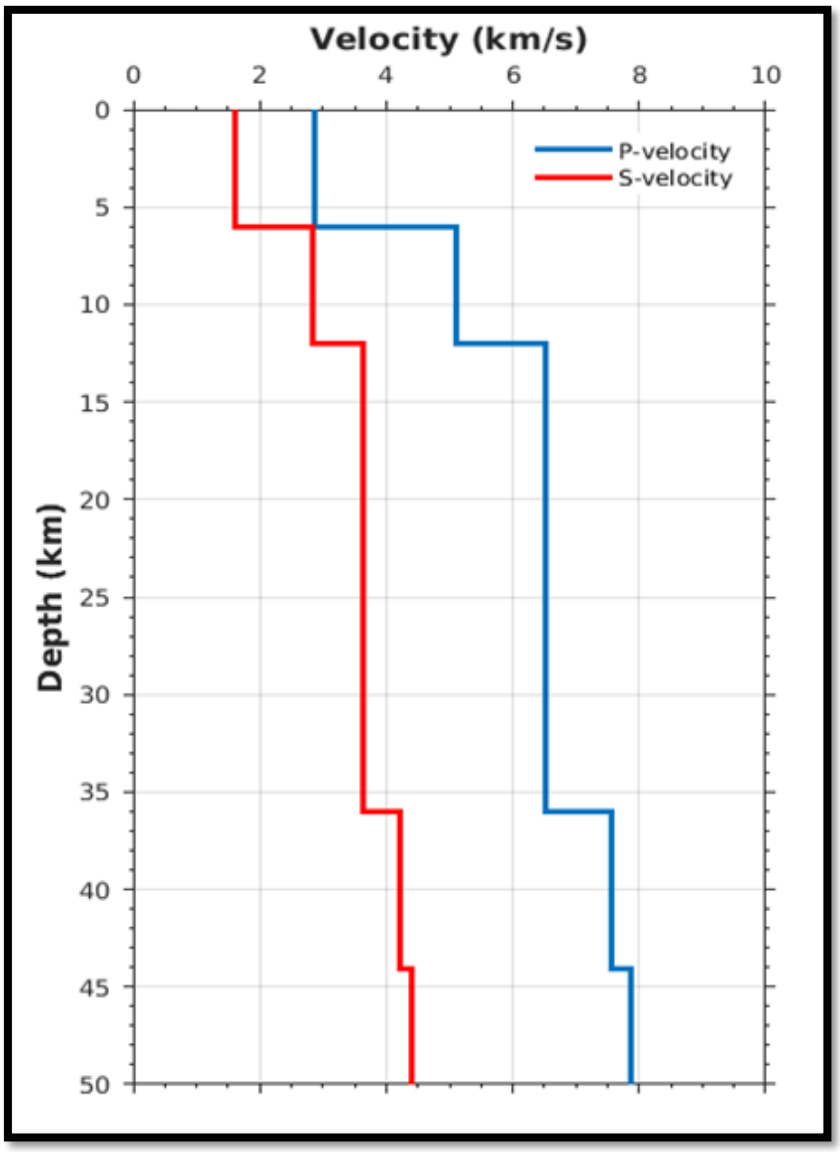

Figure 3-3: Average crustal velocity model beneath ANB1 seismic station.

Table 3-2. Crustal structure beneath ANB1 station determined from the P-wave receiver functions inversion.

Crustal Layers	Depth (km)	Vp (km/sec.)	Vs (km/sec.)	Density (gm/cm3)
Sediment 1	6	2.85	1.59	2.24
Sediment 2	6	5.08	2.83	2.51
Upper crust	24	6.51	3.63	2.84
Lower crust	8	7.55	4.21	3.16
Upper mantle	44	7.85	4.37	3.25

The best velocity model beneath KAR2 seismic station which exhibited the best matching observed and theoretical receiver functions is shown in Figure (3-4). The crustal velocity model beneath the KAR2 station is shown in Figure (3-5) and the average crustal velocity model beneath the KAR2 seismic station is shown in Figure (3-6) and listed in Table 3-3.

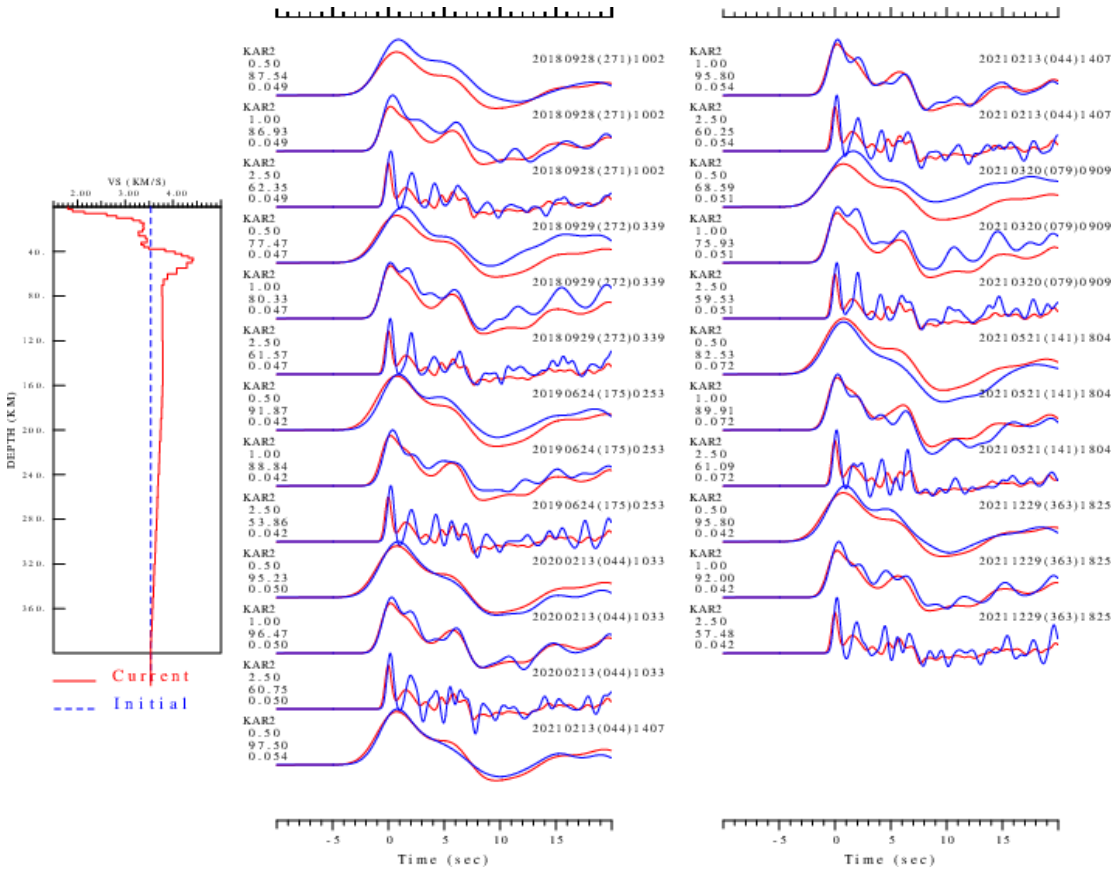

Figure 3-4: Model matching to the receiver functions of eight earthquakes recorded by KAR2. The blue curve shows the observed data and the red curve shows the model prediction.

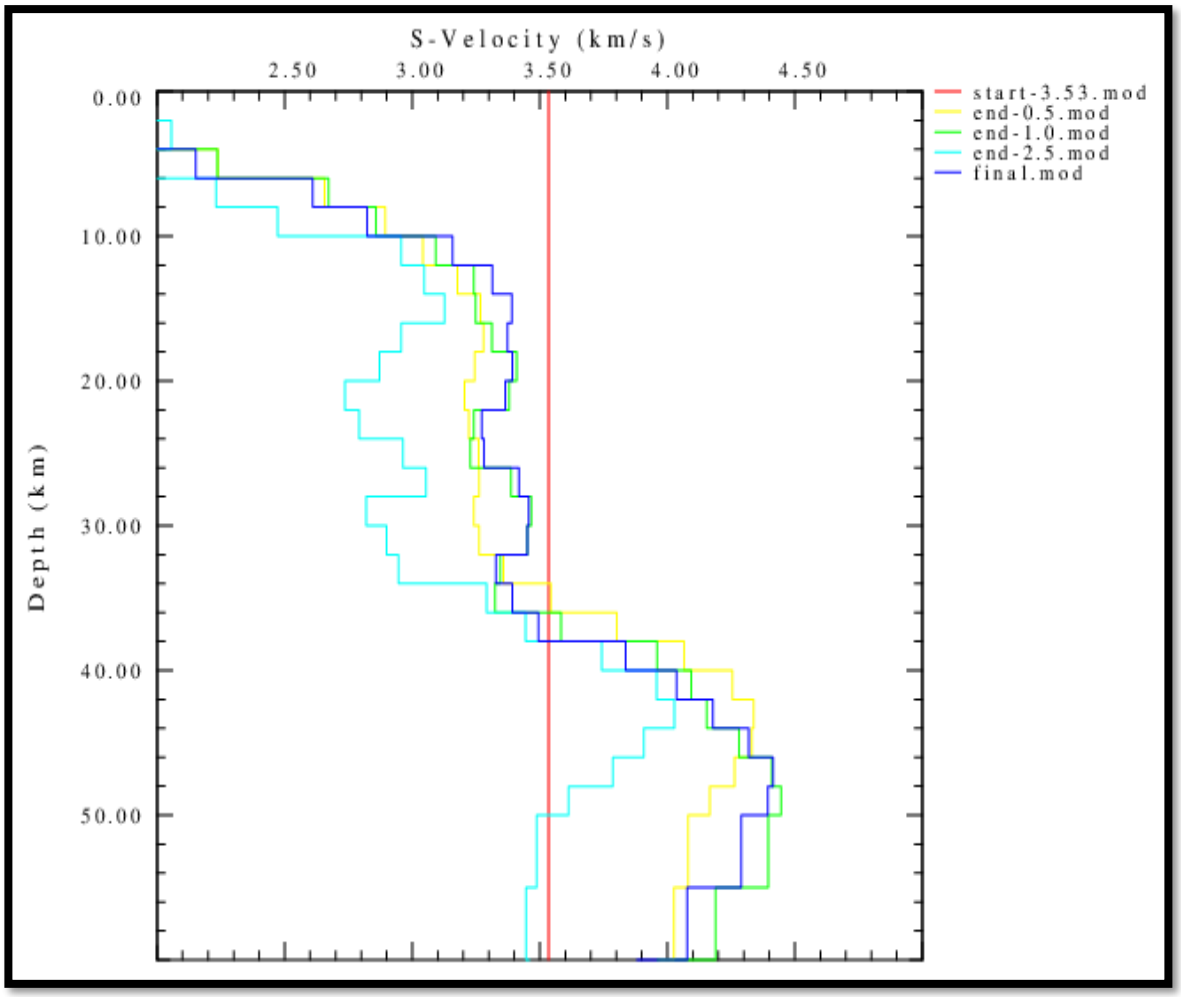

Figure 3-5 Velocity crustal model underneath KAR2 station. The red line is the starting velocity model. The blue line is the final Vs model.

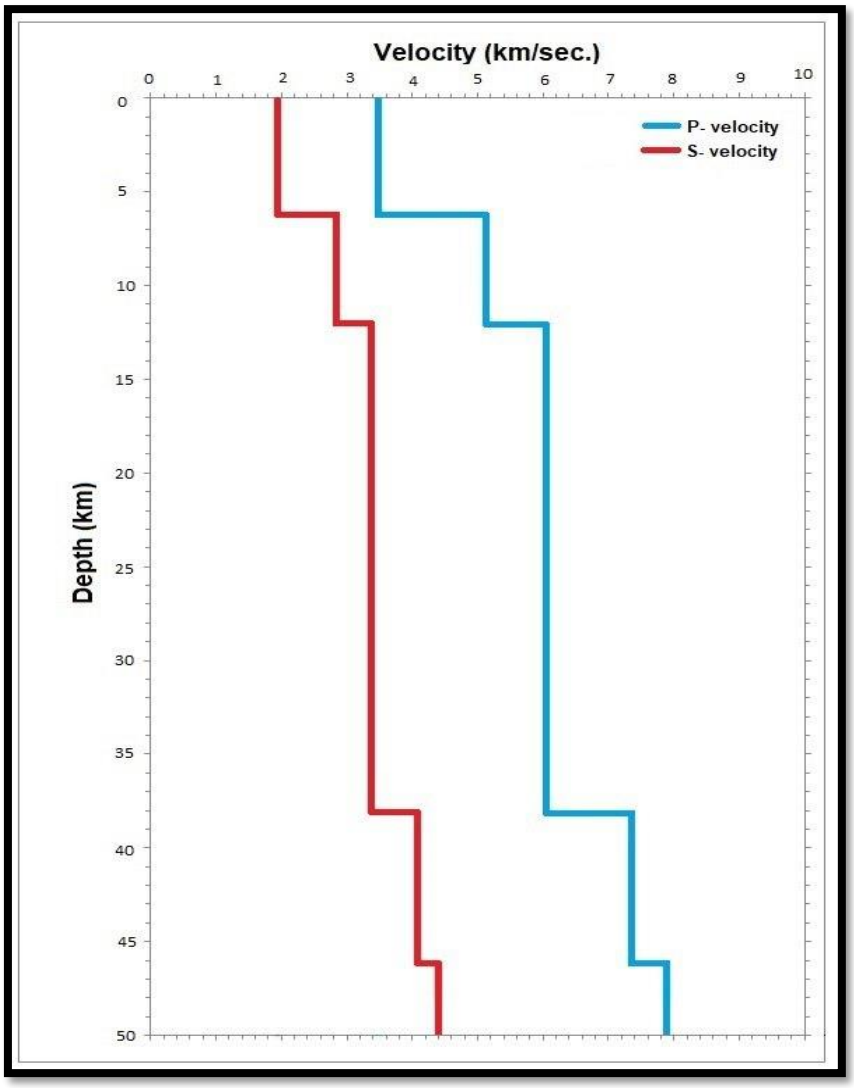

Figure 3-6: Average crustal velocity model beneath KAR2 seismic station.

Table 3-3. Crustal structure beneath KAR2 station determined from the P-wave receiver functions inversion.

Crustal	Depth(km)	Vp km/sec.)	Vs (km/sec.)	Density(gm/cm3)
Sediment 1	6	3.49	1.94	2.23
Sediment 2	6	5.13	2.86	2.52
Upper crust	26	6.05	3.37	2.72
Lower crust	8	7.33	4.09	3.09
Upper mantle	46	7.89	4.40	3.27

The crustal thickness, Vp/Vs, and Poisson's ratios are important parameters that are used to understand the crustal structure, composition, deformation and evolution. The inversion of receiver function technique was employed to determine the crustal thickness, Vp/Vs, and Poisson's ratios (σ). The receiver functions of the selected earthquakes recorded at two seismic stations, Anbar (ANB1) and Karbala (KAR2) were analyzed using the Computer Programs in Seismology (CPS). Results of inversion of the receiver functions show that the crustal thickness in the western edge of the Mesopotamian plain ranges from 44 to 46 km. The obtained crustal thickness value is consistent with that reported in the platform regions. The crustal Vp/Vs of the study area is 1.79. This value is typical for the platform region and andesitic rocks. An intermediate value (0.27) of the crustal Poisson's ratio was reported listed in Table (3-4). It indicates that there is little difference in the felsic and mafic contents of the crust.

Table 3-4. The crustal layers thickness, Vp/Vs ratio and Poisson's ratio beneath the study area.

Thick (km)	Vp (km/sec)	Vs (km/sec)	Vp/Vs Ratio	Possion's Ratio
2	2.5957	1.4478	1.7928	0.2742
2	3.0740	1.7146	1.7928	0.2742
2	3.7294	2.0820	1.7928	0.2742
2	4.6277	2.5810	1.7929	0.2743
2	5.3267	2.9712	1.7927	0.2741
2	6.0327	3.3649	1.7928	0.2742
2	6.1802	3.4471	1.7928	0.2742
2	6.2106	3.4641	1.7928	0.2742
2	6.2131	3.4659	1.7926	0.2740
2	6.3200	3.5253	1.7927	0.2741
2	6.4470	3.5959	1.7928	0.2742
2	6.4380	3.5908	1.7929	0.2743
2	6.4069	3.5738	1.7927	0.2741
2	6.4729	3.6103	1.7928	0.2742
2	6.4970	3.6238	1.7928	0.2742
2	6.5536	3.6556	1.7927	0.2741
2	6.5930	3.6440	1.7928	0.2742
2	6.7490	3.7644	1.7928	0.2742
2	6.8061	3.7963	1.7928	0.2742
2	7.1459	3.9857	1.7928	0.2742
2	7.3373	4.0924	1.7929	0.2743
2	7.4827	4.1737	1.7928	0.2742
2	7.6347	4.2583	1.7928	0.2742
2	7.7493	4.3223	1.7928	0.2742
Average	6.1093	3.4063	1.7927	0.2741

3.2. Crustal structure

3.2.1. Sedimentary cover thickness (basement depth)

The current study exhibited that the sedimentary cover thickness beneath the study area is about 12km. In other words, the basement depth is 12km. The thickness of sedimentary cover under the Karbala (KAR2) seismic station, near the ANB1 seismic station, is 11km (Abdulnaby *et al.,* 2020). The sedimentary cover thickness (basement depth) at ANB1 station is in good agreement with a value of basement depth (12km) carried out by C.G.G. (1974) using aeromagnetic data, and inconsistent with that estimated by Jassim and Goff (2006), 7km. This difference may be interpreted in terms of the resolution of the technique used in estimating the basement depth.

3.2.2. Crustal thickness (Moho depth)

The obtained results exhibited that the crust beneath the study area ranges between 44 km beneath ANB1 and 46 km beneath KAR2 with an average thickness of 45 km. thick. The study area locates on the margin of the inner unstable platform, the Mesopotamian zone. Al-Sinawi and Al-Heety (1994) Found that the average crustal thickness beneath the northern Arabian platform including the study area ranges from 35km at Rutba to 38 km at Baghdad. Al-Heety (2002) the crustal thickness determination in Iraq from long- period P-wave spectra is located in area ranges 34-36 km. The crust beneath the BHD seismic station has 43km-thick (Gök *et al*., 2008). The crustal thickness beneath the Mesopotamian plain was estimated using the receiver functions technique and the ambient seismic noise cross-correlation technique (Abdullah and Abdulnaby, 2020). They reported that the crustal thickness beneath Amara, Basrah, and Nasiriya seismic stations is 41km. The crust beneath Al-Refaei seismic station has approximately 46km-thick (Ramthan *et al*., 2020). The crustal thickness beneath a number of seismic stations distributed in the Mesopotamian plain, East of Iraq, ranges from 44km beneath the KAR2 station at the western edge of the Mesopotamian plain to about 52km beneath the AMR2 seismic station at the eastern part of the plain (Abdulnaby *et al*., 2020).The crustal thickness beneath the study area estimated by receiver functions analysis is in an agreement with the results of some previous studies (e.g. Gök *et al*., 2008; Abdulnaby *et al*., 2020). The obtained crustal

thickness value is compared to that estimated using gravity data, 30-38 km (Alsinawi *et al.,* 1987), 32-39km (Al-Banna and Al-Heety,1996). The crustal thickness value under the study area is consistent with the global average of crustal thickness in the platform regions which is equal to 39.96 ± 7.03km (Mooney *et al*.,1998).

3.1.3. Crustal Average Vp

The results showed that Vp is 6.23 km/sec in the ANB1 seismic station and 5.91 km/sec in the KAR2 seismic station. The average Vp in the study area is 6.07 km/sec. the average compressional wave velocity which approximates to the global average of crustal P-wave velocity of 6.45km/ sec (Christensen andMooney,1995). The Vp velocities in the crust of Norway increase from about 6.0 to 7.1 km/sec (Ottemoller and Midzi,2003). Average crustal in southern Korea ranged from 6.02 km/sec to 6.51 km/sec (Chang and Eob,2005). The Vp for Iraq and the northern Arabian Peninsula was from 4.50 to 4.73 km/sec (Dahham and Mohammed,1993), Al-Heety (2002) found that the average of Vp was about 6.42 km/sec and Ramthan *et al.,* (2020) found that the average of Vp is about 6.7 km/sec.

3.1.4. Crustal Average Vs

The results showed that Vs is 3.47 km/sec in the ANB1 seismic station and 3.29 km/sec in KAR2 seismic station. The average of Vs 3.38 km/sec and the average shear wave velocity which approximates the global average of the crustal S-wave velocity of 3.65 km/sec (Christensen andMooney,1995). The average shear wave velocity is 3.7 km/sec beneath the western Bengal basin (Mitra *et al.,* 2008). The Vs 3.4-3.6 km/sec beneath the N Sumatra and Malaysian peninsula (Kieling *et al.,* 2011). The shear wave velocity of 4.05 km/sec under Duhok, NW Iraq (Abdulunaby *et al.,* 2012). the crustal structure of southern Iraq the Vs range from 1.995 to 2.48 km/sec (Abdullah and Abdulunaby,2020). Ramthan *et al.,* (2020) analyzed the receiver functions to estimate the crustal model underneath Al-Refaei seismic station in central Mesopotamian Iraq (Vs= 3.62 km/sec).

3.2.3. Crustal velocity model

The crustal velocity model beneath the study area derived by the receiver functions analysis is shown in Figures (3-3 and 3-6) and listed in Tables 3-1 and 3-2. The crustal velocity model beneath the study area consists of four layers shown Figure (3-7): The first two layers represent the sedimentary cover, the third layer is the upper crust and the fourth layer is the lower crust. The velocity model shows four seismic discontinuities, the first is between the two sedimentary layers, the second one is between the sedimentary cover and upper crust, the third one is between the upper crust and lower crust and the fourth is Moho discontinuity. The depths of the first, second, third, and Moho discontinuities are 6, 12, 36, and 44km in ANB1 seismic station, 6,12,38, and 46 km in KAR2 seismic station, respectively. The obtained crustal velocity model may be employed to locate and relocate the earthquakes and in calculating moment tensor solutions in the future investigations of the study area.

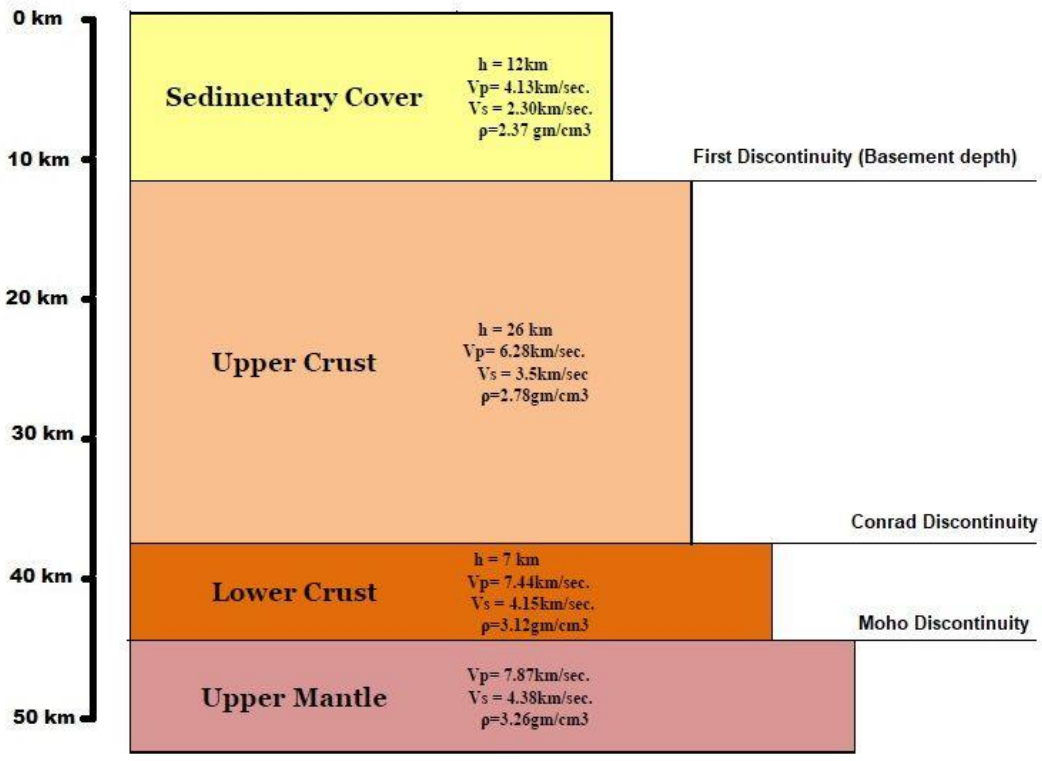

Figure 3-7: The crustal structure beneath the study area.

3.3. Geological implications of crustal structure

Crustal thickness, Vp/Vs ratio, and Poisson's ratio are important parameters to understand the crustal composition, structure, tectonic setting, and evolution (Zandt and Ammon, 1995; Zhu and Kanamori, 2000; Chevrot and Van der Hilst, 2000; Yang *et al.,* 2011). Results of the crustal thickness, Vp/Vs ratio, and Poisson's ratio beneath ANB1 and KAR2 seismic stations are listed in Table 3-4. Due to the lack of local studies related to estimating the Vp/Vs ratio and the Poisson ratio, the results of the current study will be compared are results of international studies.

3.3.1. Geological implication of crustal thickness

The crustal thickness was resulted from geological processes such as plate convergence and geological collision, serving as an important marker for defining types of global plates and regional blocks (Huang *et al.,* 2014). The thickness of the crust describes the thickening and thinning of the crust (Guo *et al.,* 2019). Tectonic deformation, thermal expansion, addition of surface volcanic products, placement of magmatic intrusions at deep inside the crust, and sedimentation all contribute to the crust thickening (Yang and Liu, 2009). Due to the ductile nature of the lower crustal layer during deformation, the crust thickens in Orogeny zones, especially in the lower crust (Condie, 2011). Lithospheric cooling, ductile flowage, subcrustal and surface erosion due to thermal uplift, injection of dense material, collapse of the magma chamber, and lateral motions such as rifting and transverse shearing all contribute to the crust thinning. (Thybo and Nielsen, 2008).

Results of inversion of the receiver functions of teleseismic earthquakes recorded by ANB1 and KAR2 seismic stations showed that the crustal thickness beneath the study area ranged from 44 to 46 km with an average value of 45 km. The crustal thickness under the study region is more than the world average continental crust thickness of 41 kilometers (Mooney, 2007). It is within range of the crustal thickness of the platform region, 39.96 ± 7.03 (Mooney *et al.,* 1998). The high thickness of sedimentary cover beneath the study area and thinning of the lower crustal layer indicate that thickening of the crust beneath the study area may be attributed to the sedimentation processes.

3.3.2. Geological implication of Vp/Vs ratio

Results of the crustal Vp/Vs ratios in the study area are listed in Table (3-5). The obtained average value of the Vp/Vs ratio beneath the study area is 1.79. This value is comparable to the worldwide average (1.78) of the continental crust and the average Vp/Vs value of the platform crust, 1.78 ± 0.01, (Zandt and Ammon, 1995; Christensen, 1996).

The Vp/Vs ratio value estimated for the study area was compared with the results of studies carried out in different regions around the world due to the lack of local studies. The obtained Vp/Vs value is higher than reported in Southern African cratons, 1.74 (Nair *et al.*, 2006), and in Australian cratons, 1.76 (Chevort and van der Hilst, 2000). The Vp/Vs average of the Iberian crust is of 1.74 ± 0.05 (Julià and Mejía, 2004). The crustal Vp/Vs ratios ranged between 1.74 and 1.83 along with the earthquake sources from Memphis, Tennessee, to St. Louis, Missouri (Catchings, 1999). In the eastern South China Block, the average crustal Vp/Vs ratio value is 1.72 (Zhang *et al.*, 2021). There is a large fluctuation of the Vp/Vs ratio value (1.68 – 1.93) in the central and western North China Craton (Wei *et al.*, 2011). In the southwestern margin of Northeast India, the crustal Vp/Vs ratio value ranges from 1.69 to 1.75 (Saikia *et al.*, 2017). The average Vp/Vs ratio value of the crust beneath South China was 1.697 (Chen *et al.*, 2019). The crustal Vp/Vs ratio beneath continental China ranged between 1.75 and 1.85 (Cheng *et al.*, 2022). In Canada, the crustal Vp/Vs ratio beneath the eastern Superior craton margins ranged from 1.66 to 1.76 except in an area dominated by anthrosite massifs is 1.85 (Vervaet and Derbyshire, 2022). In the Dominican Republic, the crustal Vp/Vs ratios vary from 1.58 to 1.99 with medium of 1.79 (Kumar et al., 2020). The crustal Vp/Vs in the western Bengal Basin, India is 1.73 (Mitra *et al.*, 2008). In the East Anatolian volcanic belt, a low average crustal Vp/Vs ratio (less than 1.71) was reported implying a felsic crustal composition at the southwest of the study region, while a high average crustal Vp/Vs ratio (1.82-1.87) was found in near volcanic centers suggesting a mafic crustal composition (AlKan, 2022).

The results of laboratory experiments and the seismic surveys have confirmed that the Vp/Vs ratio is more useful than Vp or Vs alone (Zandt and Ammon, 1995;

Christensen ,1996). The field measurements of crustal Vp/Vs ratio provide valuable constraints on crustal composition because the relation between Vp and composition is limited due to the similar P-wave velocities for many common crustal rock types (Christensen and Mooney, 1995; Christensen, 1996). The mineral composition of rocks plays a major role in the difference in Vp/Vs ratio (Christensen, 1996). There is a strong correlation between the Vp/Vs ratio value and the quartz and feldspar contents in the crust (Zhang *et al.,* 2021).

The Vp/Vs ratio value is directly proportional to the plagioclase content and inversely to quartz content (Chen *et al.,* 2010). The Vp/Vs ratio value is affected to a limited extent by the change in pressure or temperature (Christensen, 1996) and increases due to the fluid content and partial melting (Watanabe, 1993).

The study area is classified as a part of the Arabian platform area and is located on the western edge of the Mesopotamian plain (Jassim and Goff, 2006). The obtained crustal Vp/Vs value for the study area (1.79) is typical for the platform regions. The Vp/Vs ratio values for granitic, andesitic, and basaltic rocks are 1.71, 1.78, and 1.87, respectively (Tarkov and Vavakin, 1982). The calculated Vp/Vs ratio for the research area is characteristic of andesitic rocks, indicating that the crust's felsic and mafic components are differ a little.

3.3.3. Geological implication of Poisson's ratio

The Poisson's ratio is the better known crustal elastic property that is uniquely related to the Vp/Vs ratio (Chen *et al.,* 2010). The Poisson's ratio value at various crustal levels is fundamental for understanding the crustal petrology (Christensen, 1996).

The obtained crustal Poisson's ratio of the study area is 0.27. This value is consistent with the average Poisson's ratio value for the continental crust, 0.27 and with that for the platform regions, 0.27 (Zandt and Ammon, 1995). The obtained crustal Poisson's ratio value was compared with that reported in global studies. The low crustal Poisson ratio value ($\sigma = 0.249$) was reported for the Precambrian cratons in eastern China (Chen *et al.,* 2010). In East Africa, the average crustal Poisson's ratio value for all terrains of Precambrian crust is 0.25 (Tugume *et al.,* 2012). In much of northern South China, the

crustal Poisson's ratio is high (0.28–0.31), intermediate (0.26–0.29) in the eastern coastal area, extremely low (0.20–0.24) within the Jiangnan orogenic belt and around the southern coastal area, and somewhat low (0.22–0.26) elsewhere (Guo *et al.,* 2019). Across earthquake source zones from Memphis, Tennessee, to St. Louis, Missouri, the crustal Poisson's ratio ranges from about 0.26 to 0.33 (Catchings, 1999). The crustal Poisson's ratio in eastern Tibet ranges from 0.26 to 0.28 (Yang *et al.,* 2011). The crustal Poisson's ratio over mainland China is about 0.249 (Chen *et al.,* 2010).

A number of authors have interpreted the Poisson's ratio values in terms of the composition of the earth's crust (Zandt and Ammon, 1995; Christensen, 1996; Zhu and Kanamori, 2000; Ji *et al.,* 2002). They found that a low Poisson's ratio ($\sigma < 0.26$) reflects high content of felsic and low content of mafic minerals within the crust. The intermediate Poisson's ratio value ($\sigma = 0.26 – 0.28$) implies the balance contents of felsic and mafic minerals. The high crustal Poisson's ratio value ($\sigma = 0.28 – 0.30$) indicates a high content of mafic minerals and low content of felsic minerals within the crust. A Poisson's ratio greater than 0.30 was thought to indicate partial melting of rocks, a fracture zone with fluid infiltration, or a serpentinized fault zone inside the crust (Zandt and Ammon, 1995; Christensen, 1996; Ji *et al.,* 2002).

The estimated crustal Poisson's ratio in the study area ($\sigma = 0.27$) indicates that the felsic mineral content is slightly different from the mafic mineral content in the crust, which in turn, refers to the andesitic composition of the rock.

Conclusions

1. The average crustal thickness in the study area is consistent with that reported in the platform region. The thickening of the crust under the study area may be attributed to the sedimentation processes. The crustal thickness value beneath the study area is consistent with that beneath some of the seismic stations distributed in the Mesopotamian plain
2. The crustal Vp/Vs of the study area is typical for the platform region and indicates andesitic rocks.
3. The crustal Poisson's ratio of the study area indicates that there is little difference in the felsic and mafic contents of the crust
4. The basement depth (sedimentary cover thickness) beneath the study area is 12km and this value is in good agreement with the results of some previous studies and inconsistent with other studies.
5. The crustal velocity model shows four discontinuities, the first one is about 6km with Vs of 1.76 km/s, the second one is at 12km with Vs of 2.84 km/s, the third one is at 33 km with Vs of 3. km/s, and the fourth one is at depth of 45 km with Vs of 4.38km/s.

Recommendations

1. Improved estimates of crustal thickness, Vp/Vs ratio, and Poisson's ratio using the joint inversion of receiver function, surface wave dispersion, and gravity data.
2. Regionally, investigation the relationships between the crustal thickness, the Vp/Vs ratio, and Poisson's ratio for the crustal structure beneath Iraq.

References

Abdullah, R. and Abdulnaby, W. (2020) Crustal structure of southern Iraq from cross-correlation of Ambient Seismic Noise. IOSR Journal of Applied Geology and Geophysics (IOSR-JAGG), 8: 57-61.

Abdulnaby, W. G. (2013). Seismotectonics of the Northeastern Margin of the Arabian Plate in Iraq. Unpublished dissertation, Department of Applied Science of the College of Science University of Arkansas at Little Rock, US, 209P.

Abdulnaby, W., Mahdi, H., and Al-Shukri, H. (2012) Crustal Structure from Joint Inversion of Receiver Function and Surface Wave Dispersion beneath Duhok, NW Iraq. Proceedings of International Geophysical Conference and Oil & Gas Exhibition, Istanbul, Turkey.

Abdulnaby, W., Motaghi, K., Shabanian, E., Mahdi, H., Al-Shukri, H., and Gök, R. (2020) Crustal Structure of the Mesopotamian Plain, East of Iraq. Tectonics, 39, e2020TC006225. https://doi.org/10.1029/2020TC006225.

Al- Khadhimi, J.A.M., Sissakian, V.K., Fattahm A., S., and Deikran, D., B. (1996) Tectonic map of Iraq 1: 1,000,000 scale series, Publication of GEOSURV, Baghdad,sheet No. 2

Al-Banna, A.S. and Al-Heety, E.A. (1996) Crustal thickness map of Iraq deduced from gravity data. Iraqi J. Sci. 35, 749–765.

Albarède, F. (1998) The growth of continental crust. Tecthonophysics 296:1-14.

Al-Heety, E. A. (2002) Crustal structure of the northern Arabian platform inferred using spectral ratio method. Journal of Geodynamics 34 (2002) 63–75.

Alkan, H. (2022) Crustal structure in and around the East Anatolian volcanic belt by using receiver functions stacking. Journal of African Earth Sciences 191, doi: 10.1016/j.jafrearsci.2022.104532.

Alkan, H., Çinar, H., Oreshin, S., and Vinnik, L. (2019) Investigation of the crustal and upper–mantle structure of the eastern Pontides orogenic belt (NE,

Turkey): a receiver-function study. J. Seismol., https:// doi.org/10.1007/s10950-019-09818-1.

Alsinawi, S.A. and Al-Heety, E.A. (1994) Crustal thickness determination in Iraq from long-period P-wave spectra. Iraqi Geol. J. 25, 28–49.

Alsinawi, S.A., Rezkalla, I.R., and Al-Rawi, F.R. (1987) On the gravity field of Iraq. Part I. The State of the art. J. Geo. Soc. Iraq 20, 17–37.

Ammon, C.J. (1991) The isolation of receiver effects from teleseismic P waveforms, Bull. Seism. Soc. Am., 81,2504-2510.

and crustal structure, in Computer Programs in Seismology, Version. 3.30. Saint Louis University, Missouri

Annen, C., Blundy, J.D., and Sparks, R.S.J. (2006) The genesis of intermediate and silicic magmasin deep crustal hot zones. J. Petrol. 47:505–539.

Audet, P., Bostock, M. G., Christensen, N. I., and Peacock, S. M. (2009) Seismic evidence for overpressured subducted oceanic crust and megathrust fault sealing.Nature, 457, doi:10.1038/nature07650 .

Badawy, A., Hegazi, M., Gaber, H., and Korrat, I. (2018) Crustal structure of northern Egypt from joint inversion of receiver functions and surface wave dispersion velocities. *Journal of Seismology*, 22: 697-719.

Barth, M., McDonough, W. F., and Rudnick R. L. (2000) Tracking the budget of Nb and Ta in the continental crust. Chem. Geol. 165:197–213.

Buck, W. R. (1991) Mode of continental lithospheric extension, J. Geophys. Res., 96, 20,161-20,178.

C.G.G (Compagine General de Geophysique) (1974) Aeromagnetometric and Aerospectrometric survey interpretation report. (NIMCO) D.G. Geol. Surv. Min. Invest. Lib, Bagdad, Iraq.

Castro, A., Vogt, K., and Gerya, T. (2013) Generation of newcontinental crust by sublithospheric silicic-magma relamination in arcs: a test of Taylor's andesite model. Gondwana Res.23: 1554–1566.

Catchings, R. (1999) Regional Vp, Vs, Vp/Vs, and Poisson's ratios across earthquake sources zones from Memphis, Tennessee, to St.Louis, Missouri. Bull. Seism. Soc. Amer., 89: 1591-1605.

Chang, S., and Baag, C. (2005) Crustal structure in Southern Korea from joint analysis of teleseismic receiver functions and surface-wave dispersion. Bull. Seismol. Soci. Amer., 95: 1519-1534.

Chen, A., Lü, Q., Du, J., and Yan, J. (2019) The Poisson's ratio of the crust-mantle of south China and its geological significance. Geology in China 46: 750-758.

Chen, C., Lü, Q., Chen, L., Shi, D., Yan, J., and Ai, Y. (2022) Crustal thickness and composition in the South China Block: Constraints from earthquake receiver function. Science China Earth Sciences

Chen, L., Zheng, Y., Xu, Z., and Zhao, Z. (2021) Generation of andesite through partialmelting of basaltic metasomatites in the mantle wedge: Insight from quantitative study of Andean andesites. Geoscience Frontiers 12: doi: 10.1016/j.gsf.2020.12.005.

Chen, L., Zheng, Y.-F., and Zhao, Z.-F. (2016) Geochemical constraints on the origin of late Mesozoic andesites from the Ningwu basin in the Middle–lower Yangtze Valley, South China. Lithos 254: 94–117.

Chen, Y., Niu, F., Liu, R., Huang, Z., Tkalčić, H. (2010) Crustal structure beneath China from receiver function analysis. Journal of Geophysical Research 115, B03307, doi:10.1029/2009JB006386.

Cheng, S., Xiao, X., Wu, J., Wang, W., Sun, L., Wang, X., and Wen, L. (2022) Crustal thickness and Vp/Vs variation beneath continental China revealed by

receiver function analysis. Geophs. J. Int., 228: 1731-1749. Doi: 10.1093/gji/ggab433.

Chevrot, S., and van der Hilst, R. D. (2000) The Poisson's ratio of the Australian crust: geological and geophysical implications. Earth and Planetary Sci. Lett., 183: 121-132.

Chi, T., Chang, Y., and Huang, B. (2022) Receiver Function Imaging of the Crustal Structure Beneath Northern Taiwan Using Dense Linear Arrays. *Geosciences*, *12*(3): 136 ; https://doi.org/10.3390/geosciences12030136.

Chiu, J., Chiu, C., and Kim, S. (1997) The significance of the crustal velocity model in local earthquake locations from a case example of a PANDA experiment in the central United States. Bull. Seismol.- Soci. Amer., 87: 1537-1552. https://doi.org/10.1785/BSSA0870061537.

Christensen, N. I. (1996) Poisson's ratio and crustal seismology, J. Geophys. Res., 101, 3139-3156, doi:10.1029/95JB03446.

Christensen, N., and Mooney, W. (1995) Seismic velocity structure and composition of the continental crust: A global review, J. Geophys. Res., 100, 9761-9788.

Condie, K. C. (2011) Earth as an Evolving Planetary System, Second Edition, Oxford, UK, Elsevier.

Dahham, M., and Mohammed, Z.A. (1993) Crustal model for Iraq and northern Arabian Peninsula from dispersed Rayleigh waves. Abhath Al-Yarmouk: (Pure Sci. Eng.) 2, 119–134.

Durrheim, R. J., and Mooney, W. D. (1994) Evolution of the Precambrian lithosphere: Seismological and geochemical constraints. J. Geophys. Res., 99:15,359– 15,374, doi:10.1029/94JB00138.

Egorkin, A. V. (1998) Velocity structure, composition and discrimination of crustal provinces in the former Soviet Union. Tectonophysics, 298: 395-404.

Gao, S. S., Liu, K. H., and Chen, C. (2004) Significant crustal thinning beneath the Baikal rift zone: New constraints from receiver function analysis, Geophys. Res. Lett., *31*, L20610, doi:10.1029/2004GL020813.

Gök, R., Mahdi, H., Al-Shukri, H., and Rodgers, A. (2008) Crustal structure of Iraq from receiver functions and surface wave dispersion: implications for understanding the deformation history of the Arabian–Eurasian collision. Geophys. J. Int. (2008) 172, 1179–1187. doi: 10.1111/j.1365-246X.2007.03670. x.

Gómez-Tuena, A., Cavazos-Tovar, J.G., Parolari, M., Straub, S.M., and Espinasa-Pereña, R. (2018) Geochronological and geochemical evidence of continental crust 'relamination'in the origin of intermediate arc magmas. Lithos 322, 52–66.

Gómez-Tuena, A., Straub, S.M., and Zellmer, G.F. (2014) An introduction to orogenic andesites and crustal growth. Geol. Soc. Spec. Publ. 385, 1–13.

Grad, M., and Tiira, T. (2012) Moho depth of the European Plate from teleseismic receiver functions. *Journal of Seismology* **,16**: 95–105.

Guo, L., Gao, R., and Shi, L. (2019) Crustal thickness and Poisson's ratio of South China revealed from joint inversion of receiver function and gravity data. Earth and Planetary Science Letters 510: 142 – 152. doi:/10.1016/j.epsl.12.039.

Hacker, B., Kelemen, P., and Behn M. (2011) Differentiation of the continental crust by relamination. Earth Planet. Sci. Lett., 307:501–516.

Hacker, B., Kelemen, P., and Behn, M. (2015) Composition of lower crust. Annu. Rev. Earth Planet. Sci., 43: 167-205. Doi: 10.1146/annurev-earth-050212-124117.

Herrmann, R. B. (2013) Computer programs in seismology: An evolving tool for instruction and research. *Seism. Res. Lettr*., 84, 1081-1088.

Herrmann, R. B., and Ammon, C., J. (2004) Source Inversion. Computer Programsin Seismology

Herrmann, R.B. and Ammon, C. J. (2007). Surface waves, receiver functions

Herrmann, R.B., and Ammon, C.J. (2002) Computer programs in seismology, version 3.30. Saint Louis University, Missouri.

Hetenyi, G., and Bus, Z. (2007) Shear wave velocity and crustal thickness in the Pannonian Basin from receiver function inversions at four permanent stations in Hungary. *Journal of Seismology* ,11: 405–41.

http://www.eas.slu.edu/eqc/eqc_course/IntroSeis/Ass16/Ass16.pdf

Huang, H., Gue, X., Xia, S., and Qiu, X. (2014) Study of crustal thickness and Poisson's ratio in the coastal area of South China. Chinese Journal of Geophysics 57(6): 860 – 871.

Huang, Y., Chubakov, V., Mantovani, F., Rudnick, R., and McDonough, W. (2013) A reference Earth model for the heat-producing elements and associated geoneutrino flux. Geochem. Geophys. Geosyst. 14:2003–2029.

Hussien, B.M. (2012) Management of groundwater resources in Dhabaa Site using hydraulicparameters of Mullusi aquifer. Journal of Iraqi desert studies 4 :1994-7801

Jassim, S.Z., and Goff, J.C. (2006) Geology of Iraq. 1st edition, Published by Dolin, Prague and Moravian Museum, Zelny trh 6, Brno, Czech Republic. 341p.

Ji, S., Wang,Q., and Salisbury, M. (2009) Composition and tectonic evolution of the Chinese continental crust constrained by Poisson's ratio. Tectonophysics 463, 15-30. https://doi.org/10.1016/j.tecto.2008.09.007.

Julià, J., and Mejía, J. (2004) Thickness and Vp/Vs ratio variation in the Uberian crust. Geophys. J. Int., 156:59-72. doi.1111/j.1365-246X.2004. 02127.x

Kalmár, D., Hetényi, G., and Bondár, I. (2019) Moho depth analysis of the eastern Pannonian Basin and the Southern Carpathians from receiver functions. J. Seismol., 23: 967-982. https// doi.org/10.1007/s10950-019-09847-w.

Kelemen P. B. (1995) Genesis of high Mg# andesites and the continental crust. Contrib. Mineral Petrol. 120, 1–19.

Kelemen, P., Hanghøj, K., and Greene, A. (2003) One View of the geochemistry of subduction-related magmatic Arcs, with an emphasis on primitive Andesite and Lower Crust. In: Treatise on Geochemistry, Volume 3. Rudnick, R. (ed.). Executive Editors: Heinrich D. Holland and Karl K. Turekian. pp. 659. ISBN 0-08-043751-6. Elsevier, 2003., p.593-659. doi :10.1016/B0-08-043751-6/03035-8

Keller, G. R. (2013) The Moho of the North America: A Brief Review Focused on Recent Studies, Tectonophysics, doi: 10.1016/j.tecto.2013.07.031.

Kelly, A., England, R., and Maguire, P. (2007) A crustal seismic velocity model for the UK, Ireland and surrounding seas. Geophys. J. Int., 171: 1172-1184. https://doi.org/10.1111/j.1365-246x.2007.03569.x

Kent, A.J., Darr, C., Koleszar, A.M., Salisbury, M.J., and Cooper, K.M. (2010) Preferential eruption of andesitic magmas through recharge filtering. Nat. Geosci. 3: 631–636.

Kieling, K., Roessler, D., and Krueger, F. (2011) Receiver function study in northern Sumatra and the Malaysian peninsula. J. Seismol. 15: 235-259. https:// doi.org/10.1007/s10950-010-9222-7.

Koulakov, I., Gordeev, E. I., Dobretsov, N. L., Vernikovsky, V. A., Senyukov, S., and Jakovlev, A. (2011) Feeding volcanoes of the Kluchevsoy group from results of local earthquake tomography. Geophys. Res. Lett.s, 38, L09305, doi:10.1028/2011GL046957.

Kumar, S., Agrawal, Pulliam, J., Rivera, E., and Huérfano, V. (2020) Crustal thickness and bulk Poisson ratios in the Dominican Republic from receiver function analysis. Tectonophysics 775 doi: 10.1016/j.tecto.2019.228308.

Langston, C. (1979) Structure under Mount Rainier, Washington, inferred from teleseismic body waves. JGR Solid Earth 84: 4749-4762. https://doi.org/10.1029/JB084iB09p04749

Ligorria, J.P. and Ammon, C.J. (1999) Iterative deconvolution and receiver function estimation. Bull. Seismol. Soc. Am.,89:1395–1400.

Liu, K. H., and Gao, S. S. (2010) Spatial variations of crustal characteristics beneath the Hoggar swell, Algeria revealed by systematic anayles of receiver functions from a single station, Geochem. Geophys. Geosyst., *11*, Q08011, doi:10.1029/2010GC003091.

Mitra, S., Bhattacharya, S., & Nath, S. (2008) Crustal structure of the western Bengal basin from joint analysis of teleseismic receiver functions and Rayleigh dispersion. Bull. Seismol.Soci. Amer., 98:2715-2723.

Mooney, W.D. (2007) Crust and Lithospheric Structure – Global Crustal Structure. In: Seismology and the structure of the Earth., ed. by Romanowicz, Barbara and Dziewonski, Adam. Treatise on Geophysics, Elsevier, Amsterdam, pp. 361-417. DOI 10.1016/B978-044452748-6.00011-0.

Mooney, W.D., Laske, G., and Masters, G. (1998) CRUST 5.1: a global crustal model at 5o x 5o. Jour. Geo. Res., 103:727-747.

Motaghi, K., Tatar, M., Priestley, K. (2012) Crustal thickness variation across the northeast Iran continental collision zone from teleseismic converted waves. *Journal of Seismology*, 16: 253-260.

Nair, S. K., Gao, S. S0., Liu, K. H., and Silver, P. G. (2006) Southern African crustal evolution and composition: Constraints from receiver function studies. J. Geophys. Res., 111, B02304, doi:10.1029/2005JB003802.

Nawaz, M. (2019). Introductory Chapter: Earth Crust - Origin, Structure, Composition and Evolution. DOI: http://dx.doi.org/10.5772/intechopen.88100.

Niu, F., and, James, D. E. (2002) Fine structure of the lowermost crust beneath the Kaapvaal craton and its implications for crustal formation and evolution, Earth Planet. Sci. Lett., 200: 121 – 130, doi:10.1016/ S0012-821X (02)00584-8.

Nwe, L., Wei, Z., Li, Z., Bao, F., Li, X., and Hu, J. (2021) Crustal thickness, V_p/V_s ratio, and shear wave velocity structures beneath Myanmar and their tectonic implications. Earthquake Research Advances, https//doi.org/10.1018/j.eqrea.2021.100060.

Ortega, V., and D'Auria, L. (2021) Receiver function analysis for determining the crustal structure of Tenerife (Canary Islands, Spain). EGU2020-309, https:// doi.org/ 10.5194/egusphere-egu2020-309.

Ottemöller, L., and Midzi, V. (2003) The crustal structure of Norway from inversion of teleseismic receiver functions. J. Seismol., 7: 35-48.

Pondrelli S., Morelli A., Ekstrom G., Mazzaa S., Boschi E., Dziewonski A. (2002) European-Mediterranean regional centroid moment tensors: 1997–2000. Phys. Earth Planet. In., 130:71–101.

Ramthan, A., Abdulnaby, W., Abd. N., Mahdi, H., and Al-Shukri, H. (2020) Crustal structure beneath Al-Refaei seismic station- Central Mesopotamia, Iraq, using receiver function technique. Iraqi Geological Journal 53 (2A): 77-87.

Reubi, O., and Blundy, J. (2009) A dearth of intermediate melts at subduction zone volcanoes and the petrogenesis of arc andesites. Nature 461, 1269–1273.

Robertson, E. (2008) Seismic moment tensor solutions from GeoNet data to provide a moment magnitude scale for New Zealand. GNS Science. EQC. http://www.eqc.govt.nz/research/researchpapers/ seismic-moment-tensor-solutions-geonet-magnitude-scale-for-nz. Accessed Dec. 2021.

Rondenay, S. (2009) Upper mantle imaging with array recordings of converted and scattered teleseismic waves, Surveys in geophysics, 30**:** 377-405.

Rudnick R. L. (1995) Making continental crust. Nature 378, 571–578.

Rudnick, R., and Gao, S. (2014) Composition of the continental crust. In: Holland, H and Turekian, K. (eds.) Treatise on Geochemistry. 2nd ed. Elsevier 2014, pp. 1–51.

Rudnick, R.L. and Gao, S. (2003) The Composition of the Continental Crust. In: Holland, H.D. and Turekian, K.K., Eds., Treatise on Geochemistry, Vol. 3, The Crust, Elsevier-Pergamon, Oxford, 1-64. http://dx.doi.org/10.1016/b0-08-043751-6/03016-4

Saikia, S., Baruah, S., Chopra, S., Singh, U., Gogol, B., and Gohain, H. (2017) Study of crustal structure and geological implications of southwestern margin of northeast India. J. Seismol., https://doi.org/ 10.1007/s10950-017-9701-1.

Shearer, P.M. (2009) Introduction to seismology (2nd ed.). Cambridge, 396P.

Sissakian, V.K.and Muhammad, S.M. (1994) Geology of Al-Ramadi Quadrangle,GEOSURV, int. rep. no. 2315. Baghdad, Iraq.

Stein, M., and Ben-Avraham, Z. (2015) Mechanism of continental crustal growth. In: Schubert G (ed.) Treatise on Geophysics. 2nd ed. Elsevier B. V., PP. 173 – 199. Doi: 10.1016/B978-0-444-53802-4.00159-7.

Stein, S. and Wysession, M. (2003) An introduction to seismology, earthquakes, and earth structure. Malden, USA: Blackwell Publishing, 489P.

Straub, S.M., Zellmer, G.F., Gómez-Tuena, A., Espinasa-Pereña, R., Martin-del Pozzo, A.L., Stuart, F.M., and Langmuir, C.H. (2014) A genetic link between silicic slab components and calc-alkaline arc volcanism in Central Mexico. Geol. Soc. Spec. Publ. 385:31–64.

Streck,M.J., Leeman,W.P., and Chesley, J. (2007) High-magnesian andesite fromMount Shasta: a product of magma mixing and contamination, not a primitive mantle melt. Geology35: 351–354.

Taghizadeh-Farahmand, F., Sodoudi, F., Afsari, N., and Ghassemi, M. (2010) Lithospheric structure of NW Iran from P and S receiver functions. J. Seismol., 14:823-836. https:// doi.org/10.1007/s10950-010-9199-2.

Tarkov, A., and Vavakin, V. (1982) Poisson's ratio behavior in crystalline rocks: Application to the study of the Earth's interior. Phys. Earth Planet. Inter., 29:24-29, doi:10.1016/0031-9201(82)90134-0.

Tatsumi, Y., Takahashi, T., Hirahara, Y., Chang, Q., Miyazaki, T., Kimura, J.I., Ban, M., and Sakayori, A. (2008) New insights into andesite genesis: the role of mantle-derived calc-alkalic and crust-derived tholeiitic melts in magma differentiation beneath Zao Volcano, NE Japan. J. Petrol. 49:1971–2008.

Tewari, H., and Kumar, P. (2018) Velocity structure of the Indian crust. In : Tewari, H., Rajendra Prasad, B., and Kumar, P. (eds.) Structure and tectonic of the Indian continental crust and its adjoining region.2nd ed. Elsevier; 2018. P.203-209. https://doi.org/10.1016/C2016-0-04281-x.

Thybo, H., and Nielsen, C. A. (2008) Magma-compensated crustal thinning in continental rift zones, Nature, 457, 873-876.

Toiran, B. (2003) The crustal structure of Cuba derived from receiver function analysis. Journal of Seismology 7: 359-375.

Tugume, F., Nyblade, A., and Julià, J. (2012) Moho depths and Poisson's ratios of Precambrian crust in East Africa: Evidence for similarities in Archean and Proterozoic crustal structure. Earth Planetary Science Letters 355-356:73-81. Doi: 10.1016/j.epsl.2012.08.041.

Uranbaigal, P. (2014) Crustal thickness and Vp/Vs beneath the Western United States: Constraints from stacking of receiver functions. Ph.D. Dissertation. Missouri University of Science and Technology https://scholarsmine.mst.edu/doctoral_dissertations/2354.

Vervaet, F., & Darbyshire, F. (2022) Crustal structure around the margins of the eastern Superior craton, Canada, from receiver function analysis. Precambrian Research 368.https:// doi.org/10.1016/j.precamres.2021.106506.

Watanabe, T. (1993) Effects of water and melt on seismic velocities and their application to characterization of seismic reflectors. Geophys. Res. Lett., 20, 933–2936, doi:10.1029/93GL03170.

Wedepohl, K. (1995) The composition of the continental crust. Geochim. Cosmochim. Acta., 59:1217-1232.

Wei, Z., Chen, L., and Xu, W. (2011) Crustal thickness and Vp/Vs ratio of the central and western North Craton and its tectonic implications. Geophys. J. Int., 186: 385-389. doi: 10.1111/j.1365-246X.2011. 0589.x

Wessel, P., Luis, J. F., Uieda, L., Scharroo, R., Wobbe, F., Smith, W. H. F., & Tian, D. (2019). The Generic Mapping Tools version 6. *Geochemistry, Geophysics, Geosystems*, 20, 5556–5564. https://doi.org/10.1029/2019GC008515

Wever, TH., and Sadowiak, P. (1989) A relationship between crustal thickness and mean crustal velocity. Tectonophysics 170: 159-163.

Xu, L., Rondenay, S., and van der Hilst, R. D. (2007) Structure of the crust beneath southeastern Tibetan Plateau from teleseismic receiver functions. Physics of Earth and Planetary Interiors, 165, 176-193.

Yang, H., Hu, J., Li, G., Zhao, H., Wen, L. (2011) Analysis of the crustal thickness and Poisson's ratio in eastern Tibet from teleseismic receiver functions. Geophys. J. Int., 168:1380-1388. https://doi.org/ 10.1111/j.1365-246X.2011. 05118.x

Yang, Y., and Liu, M. (2009) Crustal thickening and lateral extrusion during the Indo-Asian collision: A 3D viscous flow model, Tectonophysics, 465, 128-135.

Yass, A.M., Hussein, K.T.and Tawffeq, S.K.(2016) Qualitative Interpretation of the Airborne Radiometric Dataof H1 Quadrangles using GIS Techniques, GEOSURV Library, int.rep.no.3603, Baghdad,Iraq.

Yu, Y., and Hua, L. (2021) Crustal thicknesses and V_P/V_S ratios beneath South China estimated from receiver function analysis and their geological implications. *Chinese Journal of Geophysics* ,64 : 146-156.

Zandt, G., and Ammon, C. J. (1995) Continental crust composition constrained by measurements of crustal Poisson's ratio, Nature, 374, 152-154.

Zhang, J., Chen, L., and Wang, X. (2019) Crustal structure study based on principal component analysis of receiver functions. *Science China Earth Sciences* **, 62**: 1110–1124.

Zhang, Y., Shi, D., Lu, Q., Xu, Y., & Xu, Z. (2021) The crustal thickness and composition in the eastern South China Block constrained by receiver functions:

Implications for geological setting metallogenesis. Ore Geology Reviews 130. https:// doi.org/ 10.1016/j.oregeorev.2021.103988.

Zhou, R., Stump, B., Herrman, R., Yang, Z., and Chen, Y. (2009)Teleseismic receiver function and surface-wave study of velocity structure beneath the Yanqing-Huailai basin northwest of Beijing. Bull. Seis. Soci. Amer., 99:1937-1952.

Zhu, L., and Kanamori, H. (2000) Moho depth variation in Southern California from teleseismic receiver functions, J. Geophys. Res., 105, B2: 2969-2980.

المستخلص

تهدف الدراسة الحالية إلى التعرف على المضامين الجيولوجية لبنية القشرة تحت محطتين زلزاليتين في وسط العراق، حيث تم استخدام انعكاس دوال المستقبل للموجة الانضغاطية لتحديد بنية القشرة تحت محطتي الأنبار وكربلاء الزلزالية. تم استخدام بعض برامج الكمبيوتر في علم الزلازل (CPS) لتحليل وظائف المستقبل لسبعة عشرة هزة أرضية بعيدة.

أظهرت نتائج انعكاس دوال المستقبل أن سمك القشرة (عمق موهو) تحت منطقة الدراسة يتراوح من 44 إلى 46 كم بمتوسط قيمة 45 كم. تبلغ سماكة الغطاء الرسوبي (عمق صخور القاعدة) في منطقة الدراسة حوالي 12 كم. بشكل عام ، سمك الغطاء الرسوبي الذي تم الحصول عليه وسماك القشرة الأرضية متوافقة مع نتائج بعض الدراسات السابقة في سهل الحوض الرسوبي.

بالإضافة إلى أن نتائج الانعكاس أوضحت أن نموذج سرعة القشرة تحت منطقة الدراسة يتضمن أربع انقطاعات مميزة ؛ الأول عند 6 كم مع 1.76 كم / ثانية ، والثاني عند 12 كم مع 2.84 كم / ثانية ، والثالث عند 33 كم مع 3.50 كم / ثانية ، والرابع عند 45 كم مع 4.15 كم / ثانية. يمكن استخدام نموذج السرعة الذي تم الحصول عليه لتحديد موقع الزلازل المحلية والبعيدة ونقلها وفي حلول مستوى الصدع.

ان سمك القشرة، ونسبة سرعة الموجة الانضغاطية الى الموجة القصية، ونسبة بواسون هي معاملات مهمة تستخدم لفهم بنية القشرة وتركيبها الكيمياوي وتشوهها وتطورها. كما ذكرنا سابقاً فإن سمك القشرة الأرضية لمنطقة الدراسة يتراوح من 44 إلى 46 كم. تتوافق قيمة سمك القشرة التي تم الحصول عليها مع تلك التي تم سجلت في مناطق المنصة. أظهرت الدراسة أن قيمة نسبة سرعة الموجة الانضغاطية الى سرعة الموجة القصية لمنطقة الدراسة تساوي 1.79. هذه القيمة نموذجية لمنطقة المنصة والصخور الأنديساتية. تم تسجيل قيمة متوسطة (0.27) لنسبة بواسون للقشرة الأرضية تحت منطقة الدراسة والتي تدل على وجود اختلاف بسيط في محتويات صخور القشرة الحامضية والقاعدية.

جمهورية العراق
وزارة التعليم العالي والبحث العلمي
جامعة الانبار/كلية العلوم
قسم الجيولوجيا التطبيقية

المضامين الجيولوجية لتركيب القشرة في وسط العراق باستخدام طريقة دالة المستقبل

رســـــالة

مقدمة إلى مجلس كلية العلوم/ جامعة الانبار وهي جزء من متطلبات نيل درجة الماجستير في الجيولوجيا التطبيقية

من قبل

هــدى فرحان رافع

بكالوريوس جيولوجيا التطبيقية / كلية العلوم/ جامعة الانبار (2019)

بإشراف

أ. د عماد عبد الرحمن محمد صالح

كلية العلوم – جامعة الانبار

أ.م. د. واثــق عبد النبي

جامعة البصرة-كلية العلوم

1443 هـ 2022م